Heating ability modulation by clustering of magnetic particles for precision therapy and diagnosis

Heating ability modulation by clustering of magnetic particles for precision therapy and diagnosis

Gabriele Barrera, Paolo Allia and Paola Tiberto

INRIM, Advanced Materials Metrology and Life Sciences, Strada delle Cacce 91, 10135 Torino, Italy

E-mail: g.barrera@inrim.it

February 2021

Abstract. Magnetic and thermal properties of clustered magnetite nanoparticles submitted to a high-frequency magnetic field is studied by means of rate equations. A simple model of large particle clusters (containing more than one hundred individual particles) is introduced. Dipolar interactions among clustered particles markedly modifiy shape and area of the hysteresis loops in a way critically dependent on particle size and cluster dimensions, thereby modulating the power released as heat to a host medium. For monodisperse and polydisperse systems, particle clustering can lead to either a significant enhancement or a definite reduction of the released power; in particular cases the same particles can produce opposite effects in dependence of the dimensions of the clusters. Modulation by clustering of the heating ability of magnetic nanoparticles has impact on applications requiring optimization and accurate control of temperature in the host medium, such as magnetic hyperthermia for precision therapy or fluid flow management, and advanced diagnostics involving magnetic tracers.

1. Introduction

The interest towards the high-frequency properties of magnetic nanoparticles has substantially increased with the rise of applications of magnetically driven particles as sources of heat or contrast agents. Applications include such different areas as biomedicine [1] and oil extraction and transportation industry [2] where, despite the diversity of subjects, basically the same language, methods, and physical parameters are involved.

In biomedicine, the functional properties of magnetic nanoparticles play an important role in rapidly evolving techniques for precision therapy [3] and diagnosis, such as Magnetic Hyperthermia (MH) [4] where particles serve as point-like heat sources around or inside internal organs of living bodies, and Magnetic Particle Imaging (MPI) [5] where they act as magnetic tracers. In both cases, modulating in a controlled way the heating power released by particles to the surrounding tissues is mandatory in order to

achieve an efficient, non damaging therapeutic practice or visualization. In MH the aim is usually to maximize the heating ability of magnetic particles whereas in MPI, where particles serve as non-invasive, diagnostic tracers, the released power should usually be kept as low as possible.

Magnetic hyperthermia has been introduced in the clinical practice as a precision therapy aimed to inflict damage to malignant cells by means of the heat generated by nanoparticles containing transition-metal atoms or ions. The nanoparticles, which must be as biocompatible as possible [6], are submitted to a magnetic field H of high frequency (typically in the interval 10 kHz$\leq f \leq$1 Mhz) and suitable amplitude [7] with harmonic or non-harmonic time behaviour [8, 9]. Human physiology imposes limits on the physical parameters of operation; in particular, the product Hf cannot exceed an upper threshold in order to avoid discomfort or even nuisance to patients [10]. MH can be exploited either as a standalone therapy [11] or in association with other curing techniques, such as chemotherapy or radiotherapy [12]; in this case, the heat released by magnetic nanoparticles favours a higher therapeutic efficacy and a deeper malignant tissue penetration [13].

In MPI, the magnetic signal from nanoparticles excited by a high-frequency harmonic field allows the users to determine their spatial distribution inside vessels or tissues by means of a tomographic procedure [14]. Medical applications include vascular imaging and visualization of internal organs, MPI being a promising alternative to techniques such as positron emission tomography and single-photon computed tomography which make use of radioactive tracers [15]. Although in some cases it could be advantageous to associate heating to tracing, in general MPI is intended to work as a diagnostic method with very limited or no impact on tissues or vessels. In this case, release of heat to the environment may be an undesired by-product of nanoparticle magnetic excitation. The short duration of a particle's excitation is often considered to guarantee that heating effects are negligible, although there is some controversy about this point, as well as indications that the problem may be underestimated [16]. Diagnostic MPI requires minimizing the heat released by excited nanoparticles.

Other biomedical applications, based on the displacement of particles by effect a magnetic field rather than on heating effects include blood detoxification by magnetic separation [17, 18] and magnetically-assisted haemodialisis [19]. In all cases involving the interaction of particles with living bodies, bio/haemocompatibility and biodegradability of magnetic particles play a most important role, as pointed out for various types of bare, coated, protein-conjugated magnetite nanoparticles [20, 21, 22, 23, 24, 25]

A radically different area of application of the heating properties of magnetically excited nanoparticles is the treatment of fluids in oil extraction industry (e.g., water-based/oil-based drilling fluids) and the active coating of the inner surfaces of tubing to eliminate hindrances to steady flow of oil (dewaxing). The heat delivered by the magnetic nanoparticles [2, 26] is exploited for flow assurance and improved production and transport of heavy oil.

In all these cases, an in-depth knowledge of the physical effects underlying the production of energy by magnetic nanoparticles is mandatory. Despite the ample literature on power generation by magnetically driven particles, this aim is still far from being accomplished. So far, expressions for the generated power based on the linear response theory [27] have been widely used; however, often the experimental or theoretical conditions do not allow one to freely make use of such an approximation [28]. At the present stage of scientific development, paralleled by a process of standardization of the techniques [28, 29, 30, 31], it is necessary to go beyond simplified theories by exploiting a more precise description of the physical mechanisms which govern the generation of energy by magnetic nanoparticles in order to obtain reliable predictions impacting present-day applications.

An important step forward towards a complete understanding of the processes leading to the production of heat by magnetization rotation or reversal in nanoparticles is based upon the recognition of the inherent complexity and non-linearity of the underlying physical effects which require to be studied from a physicist's standpoint [32].

In this work, a strategy aimed to modulate the ability of magnetic nanoparticles to release heat to an environment is proposed and discussed. We show that in the presence of dipole-dipole interaction nanoparticle clusters either enhance or reduce the released power with respect to a homogeneous distribution of particles, the fundamental parameters which determine the sign of the effect being the size of the nanoparticles and/or the dimensions of the clusters.

A simple model of compact (i.e., three-dimensional, non-dendritic) particle clusters is proposed. The average distance of individual nanoparticles inside a cluster is smaller than in the case of a homogeneous dispersion, so that dipole-dipole interaction among individual particles cannot be neglected. This paper is focussed on clusters with size of the order of some hundreds of nanometers containing from many hundreds to a few thousands particles. Examples of this type are not uncommon in the recent literature [33, 34, 35, 36, 37, 38, 39, 40, 41]. In this case, no direct simulation of the system by means of computational algorithms (e.g., by solving the LLG equations [42] or by using Monte-Carlo methods [43]) is possible, whereas this in the natural playground for an approximate approach based on rate equations [44, 45].

The effect of dipole-dipole interaction within a cluster is studied in the rate-equation framework by using a recent theory where the interaction is described as an additional contribution to the energy barrier between the two easy directions for the particle's magnetic moment [45, 46]. Rate equations determine the time evolution of the magnetization when the particles are excited by a high-frequency field, and allow one to draw the magnetic hysteresis loops. The loop area is proportional to the magnetic power released to the environment as heat.

The model predicts the changes of the hysteresis loops of clustered particles of magnetite (Fe_3O_4) which take place when the cluster size is ideally changed (magnetite nanoparticles are nowadays one of the most commonly used therapeutic agents in

nanobiomedicine owing to their biocompatibility). Monodisperse particles (i.e., all having the same size) with randomly distributed easy directions are studied first. It is shown that densely populated clusters are able to release an amount of thermal power markedly different from the one generated by homogeneous distributions. The same behaviour is observed not only for monodisperse nanoparticles but also in polydisperse systems, provided that the size distribution function is not too wide.

Therefore, the amount of released heat can be modulated, depending on one's needs and the specific application, by using fluid carriers or materials containing properly clustered instead than individual magnetic nanoparticles.

2. Model

2.1. Rate equations and dipolar interaction model

Rate equations have been shown to be particularly effective in the study of the behaviour of magnetic nanoparticles submitted to a magnetic field in the low to intermediate radio-frequency region ($f < 1$ MHz) [45, 47, 48]. In the rate-equation framework, the particles are viewed as classical two-well systems characterized by uniaxial magnetic anisotropy with randomly distributed easy axes. A summary of the distinctive features of this approach is found in the Supplementary Material (Section 1). The particles are assumed not to be physically displaced or rotated by effect of the driving field, as typically observed at high frequency and inside living bodies [49].

The dipolar interaction among nanoparticles is taken into account by adding a term to the standard expression of the energy barrier between the two wells, therefore approximating a multi-body problem in terms of a single-particle, mean-field theory, as discussed elsewhere [47, 50]. For particles made of magnetite (Fe_3O_4) with volume $V = \pi/6\, D^3$, D being the particle's diameter and magnetic moment $\mu = M_s V$ (M_s=350 kA/m [=350 emu/cm^3] being the saturation magnetization at room temperature) dispersed in a diamagnetic host, the maximum value of the additional contribution E_D^{max} to the local energy barrier of each particle is‡:

$$E_D^{max} = \frac{\mu_0}{4\pi}\,\alpha\frac{\mu^2}{d_0^3} = \frac{\mu_0}{4\pi}\,\alpha M_s^2 V \frac{V}{d_0^3} = \frac{\mu_0}{4\pi}\,\alpha M_s^2 V\, f_V \qquad (1)$$

where d_0 is the average interparticle distance, related to the volume fraction of particles dispersed in the host medium by the relation $f_V = V/d_0^3$ [45], and α is a numerical constant of the order of 10 deriving from the sum over the contributions of magnetic dipoles surrounding each particle [51]. The maximum value of the dipolar energy is attained when the dipoles are pointing towards all directions in space during a cyclic magnetization process (i.e., when the net magnetization of the material is equal to zero, corresponding to the coercive field on the hysteresis loop). When the dipoles are aligned by the applied field H, the dipolar energy takes a smaller value [52]; this

‡ in SI-units; equations in cgs-units are reported in the Supplementary Material, Section 8.

has been modelled by introducing an *ad-hoc* term in the expression of E_D [45], which finally becomes:

$$E_D(H) = \frac{\mu_0}{4\pi}\ \alpha M_s^2 V\,(1 - \frac{|m_0|(H)}{2}) f_V \tag{2}$$

where the alignment parameter $|m_0| = |M_0|/M_s$ is the absolute value of the reduced magnetization of a non-interacting system of monodisperse particles with random easy axes. This dimensionless quantity takes values between 0 and 1, being zero at the coercive field and unity at magnetic saturation ($H \to \infty$); when $H = 0$ it corresponds to the reduced remanence of the non-interacting loop. The above expression holds for ideally homogeneous or nearly-homogeneous nanoparticle systems.

The energy barrier $E_{B\,i}(H, \phi)$ of a two-well system whose easy anisotropy axis makes an angle ϕ with the magnetic field becomes therefore:

$$E_{B\,i}(H, \phi) = E^0_{B\,i}(H, \phi) + \frac{\mu_0}{4\pi}\ \alpha M_s^2 V\,(1 - \frac{|m_0|(H)}{2}) f_V. \tag{3}$$

$E^0_{B\,i}(H, \phi)$ is the height of the barrier for a non-interacting particle (as seen from potential well i, with i =1,2) and contains the product of the material's magnetic anisotropy K_u (2×10^4 J/m^3[$= 2 \times 10^5$ erg/cm^3] at room temperature for magnetite) times the volume V [46], so that the total energy barrier is directly proportional to the particle volume. The quantity $E^0_{B\,i}$ depends on angle ϕ when $H \neq 0$, by effect of the coupling energy term between particle's magnetic moment and the external field. The modified energy barrier regulates the time of jump of individual particles from one well to the other. The hysteretic magnetization is then obtained for each ϕ angle, and the $\phi-$dependent results are finally averaged over all angles between the anisotropy axis and the magnetic field [44].

In homogeneous systems, the effect of dipolar interaction is complex: the additional energy term, very sensitive to particle size and interparticle distance, turns out to either increase or decrease the area of the hysteresis loops generated in real applications [45, 53], therefore acting to enhance or reduce the thermal efficiency of an assembly of interacting nanoparticles.

The actual interval where magnetite particles excited at high frequency are able to generate a substantial amount of heat in typical operating conditions of *in vivo* applications is not particularly extended, being approximately in the 13-18 nm interval [47]. In fact, the constraints imposed by physiology require applying small fields when high frequencies are used in order to keep the product Hf sufficiently low [10], so that as a rule the particles are called to describe a *minor* hysteresis loop, i.e., one where the maximum magnetization (i.e., the magnetization measured at $|H_V|$) is very far from technical saturation.

It should be noted that in *major* hysteresis loops (where the maximum magnetization is at or very close to technical saturation), the loop's area is basically dominated by the coercive field $H_c^{(maj)}$, which at high operating frequency monotonically increases

with increasing particle size (see Supplementary Material, Section 2). On the contrary, the area of minor high-frequency loops is substantially different from zero only when the vertex field is of the same order of magnitude as the coercive field of the major loop, i.e., $H_c^{(maj)} \simeq H_V$ [45]. There is a limited interval of particle sizes where this condition is fulfilled; for values of D outside this interval, the loops are very narrow and the associated area very small. The point is made clear in the Supplementary Material.

In a polydisperse system characterized by a distribution function of particle sizes $p(D)$ and a random distribution in space of particles having different sizes, with average interparticle distance $\overline{d_0}$, Equation (3) is substituted by [45]:

$$E_{B\,i}(H,\phi) = E^0_{B\,i}(H,\phi) + \frac{\mu_0}{4\pi}\,\alpha M_s^2 \frac{\overline{V^2}}{\overline{V}}\,(1 - \frac{\overline{|m_0|}(H)}{2} f_V, \tag{4}$$

where $\overline{V} = \int V p(D) dD$, $\overline{V^2} = \int V^2 p(D) dD$, and use has been done of the relation $f_V = \overline{V}/\overline{d_0}^3$. The dipolar energy is still given by Equation (1) where $\mu^2 \to \overline{\mu^2} = M_s^2 \overline{V^2}$. Here $\overline{|m_0|}$ is the absolute value of the average reduced magnetization of size-distributed, non-interacting particles. The resulting hysteresis loops are first averaged over ϕ and finally summed up using $p(D)$ as weight function.

As a final remark, the rate equation approach cannot be indiscriminately exploited to describe the behaviour of magnetic nanoparticles of arbitrary size [8]. In principle, rate equations approximate the Fokker-Planck equation for the double-well problem when the ratio $E_{B\,i}/k_BT$ is larger than unity [54]; however, they were shown to be still useful when $E_{B\,i}/k_BT \simeq 0.92$ or just below [54]. As a consequence, at each temperature there is a lower limit to the diameter of nanoparticles which can be analysed by the rate equation method. Taking $E_{B\,i} = E^0_{B\,i} = K_u V$, the limit is expressed by the condition $D \gtrsim (5.52\, k_BT/\pi K_u)^{1/3}$. In the present case, around room temperature the lower limit turns out to be $D \simeq 7.5$ nm, so that the diameter D of the studied particles is equal to or larger than 8 nm.

2.2. Modeling nanoparticle clusters

We study the effect of inhomogeneities in the space distribution of magnetic particles on the hysteresis loops and the resulting heating efficiency, without however investigating the microscopic causes leading to the development of inhomogeneities (which can be of electrical, magnetic, chemical nature). Inside a cluster the magnetic particles are assumed to be still isolated, i.e. not in physical contact (in order to exclude magnetic contact interaction such as the exchange interaction); however, the interparticle distance d is much shorter than the one existing in a homogeneous system with the same volume fraction, so that the dipole-dipole energy, proportional to d^{-3}, is much stronger. On the other hand, clusters are assumed to be well separated from each other, so that dipolar interactions between any two of them can be neglected as a first approximation.

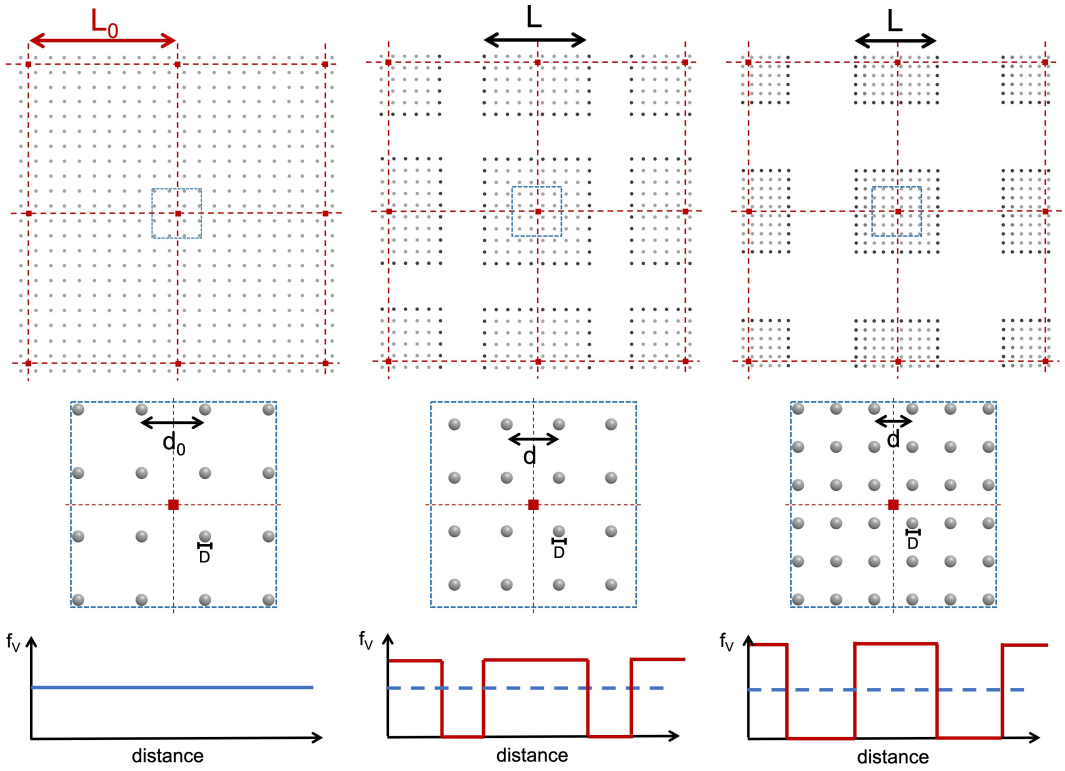

Figure 1. Two-dimensional sketch of idealized particle clustering. Each dot of the array represents a magnetite nanoparticle of diameter D. Left panel: uniform distribution of particles with mean distance d_0. Centre and right panels: two different stages of the formation of clusters of side L. The second row shows for all cases an enlargement of the region outlined in blue in the first row. The behaviour of the density of particles is schematically shown in the third row.

We consider monodisperse particles first. The development of clusters from an initially homogeneous distribution of particles is figured out as follows (see Figure 1, where for simplicity the two-dimensional case is depicted):

- homogeneously dispersed particles of diameter D are first placed on a simple cubic lattice whose nearest-neighbour distance is $d_0 = (V/f_V)^{1/3}$ (upper left panel of Figure 1; the intermediate left panel shows an enlarged view of the immediate surroundings of any particle);
- the length $L_0 = Nd_0$ is introduced, with $N >> 1$ (two cases [$N = 10$ and $N = 20$] will be considered in the following); the system of nanoparticles can therefore be viewed as an assembly of juxtaposed, identical cubes of side L_0; the length L_0 is linked to the number of particles in a cluster, $N^{(cl)} = (N+1)^3 \simeq L_0^3 f_V/V$;
- the size of each cube is then uniformly reduced along three dimensions by keeping the initial distance between centres (L_0); the side length becomes $L < L_0$ (centre panels of Figure 1); within a cluster the interparticle distance is now $d < d_0$, with $d = L/N$;

- during the process the center-to center distance between adjacent clusters remains fixed at L_0;
- the process is carried on until a minimum interparticle distance is attained (right panels of Figure 1);
- the cubic clusters are assumed to be separated by a face-to-face distance $L_0 - L$ such that they can be considered as non-interacting. This means that the actual arrangement of the clusters within the material is unimportant, i.e., the model's results do not depend on the more or less regular separation between clusters;
- the *average* density of particles in the host material (parameterized by the volume fraction f_V) is always the same and equal to V/d_0^3; however, within a cluster the local density becomes $f_V^{(cl)} = V/d^3$ while outside it drops to zero, each cluster being surrounded by a region of material where there are no particles; this is schematically shown (in one dimension) in the bottom line of Figure 1.

We explicitly acknowledge that this highly idealized mechanism of particle clustering is not a description of the actual processes of cluster formation in real materials, which are usually driven by physical or chemical mechanisms including interaction with hydrophobic blocks of copolymers [33, 41] or microgels [34, 38], alternating magnetic field assisted co-precipitation [35], solvothermal reactions [36] and surfactant-assisted synthesis [37]. However, our model has the advantage of providing a simple way to understand how and how much does dipolar interaction affect the magnetic behaviour of clusters of different size. Using a different spatial arrangement of nanoparticles does not to entail substantial differences with respect to this model (see Supplementary Material, Section 3).

These cubic particle clusters contain $(N+1)^3$ particles whose distance is lower than d_0 and are separated by extended regions of non-magnetic material. The model can be applied to describe the magnetic properties of arrays of dense, isotropic clusters of particles, often observed in the literature [33, 34, 35, 36, 37, 38, 39, 40, 41], whilst cannot be directly applied to describe irregular or fractal clusters [55] or linear chains [56].

Both an upper and a lower limit to cluster size can be defined. The lower limit of L derives from the requirement that the dipolar energy should not exceed a maximum threshold in order to apply the mean-field approach of Equations 1 and 2. In particular, the maximum dipolar energy defined in Equation 1 must not be much larger than the barrier arising from the particle's magnetic anisotropy [57], which is equal to $K_u V$ when $H = 0$. Requiring that $E_D^{max} \lesssim 2\,K_u V$ implies that the condition $\frac{\mu_0}{4\pi}\alpha M_s^2 f_V \lesssim 2\,K_u$ must be satisfied; this results in the following condition on the interparticle distance d:

$$d \gtrsim d_{min} = \left(\frac{\mu_0\,\alpha M_s^2}{48 K_u}\right)^{1/3} D \tag{5}$$

With the parameter values used in this work, the condition becomes $d \gtrsim 1.17\,D$. As a consequence, we require that d not to be less than $d_{min} = 1.2\,D$, so that $L \geq 1.2\,N D$.

The upper limit of L derives instead from the requirement that the clusters must

be separated from each other so that the dipolar interaction between any two of them is negligible. The existence of an effective cutoff length for dipole-dipole interactions among magnetic nanoparticles has been inferred by theoretical considerations [45] and substantiated by measurements [58, 59]. In particular, the cutoff length λ is of the order of $4\,D$ at f =100 kHz, i.e., at the magnetizing frequency used in this work [45]. In other words, magnetic particles separated by a distance equivalent to four diameters or more can be assumed as non-interacting. An explicit proof can be found in the Supplementary Material, Section 4. It is therefore required that two neighbouring cubes of size L are placed at a face-to-face distance such that $L_0 - L > 4\,D$, which can be transformed into the condition $d < d_{max} = d_0 - 4D/N$.

In the following, the model will therefore be applied by requiring that the interparticle distance within a cluster d varies in the range $1.2\,D \leq d \leq (d_0 - 4D/N)$.

2.3. Dipole-dipole interaction in a cluster

Within a cluster, the dipole-dipole interaction is generally enhanced by the reduction of the interparticle distance. However, a distinction has to be made between core and surface effects. In fact, particles present, e.g., on the cube's face experience a reduced dipolar interaction because of the lack of translational symmetry. An example is shown in Figure 2, where the left panel refers to a particle in the cluster's core and the right panel to a particle on any of the cube's faces. In both cases, the reference particle (in red) is surrounded by magnetic dipoles placed on the $1^{st}, 2^{nd}, 3^{rd}$ ... neighbour lattice sites and concurring to determine the value of the dipole-dipole energy on it. For simplicity of representation, only the first three neighbours are highlighted in different colours. The actual counting of active neighbours takes into account the requirement that their distance from the centre has to be smaller than $\lambda = 4\,D$, as previously discussed; it should be noted that the actual number of dipoles giving a nonzero contribution to the dipolar energy increases with reducing the cluster size, i.e., the inner interparticle distance d.

The dipole-dipole energy of a core particle (panel *a*) and of a particle placed either on a face (as in panel *b*), or an edge or a vertex of the cube is assumed to be determined by the number of active neighbours, which is different in each case (core, face, edge, vertex). The assumption can be justified by recalling that the parameter α appearing in Equation 1 actually contains a summation over all active neighbours [51] of the reference particle.

Therefore, if the number of active neighbours for a particle placed on a cube's face is n_f and the one for a core particle is n_c, with $n_f < n_c$, the dipolar energy on the former particle is assumed to be simply reduced by a factor n_f/n_c with respect to the one of a core particle. It should be noted that a decrease in the number of active neighbours is observed not only for the particles on the outer layer of the cube, but also for the ones present on the second layer from outside.

As a consequence, the energy barriers are different for two-level systems in the core

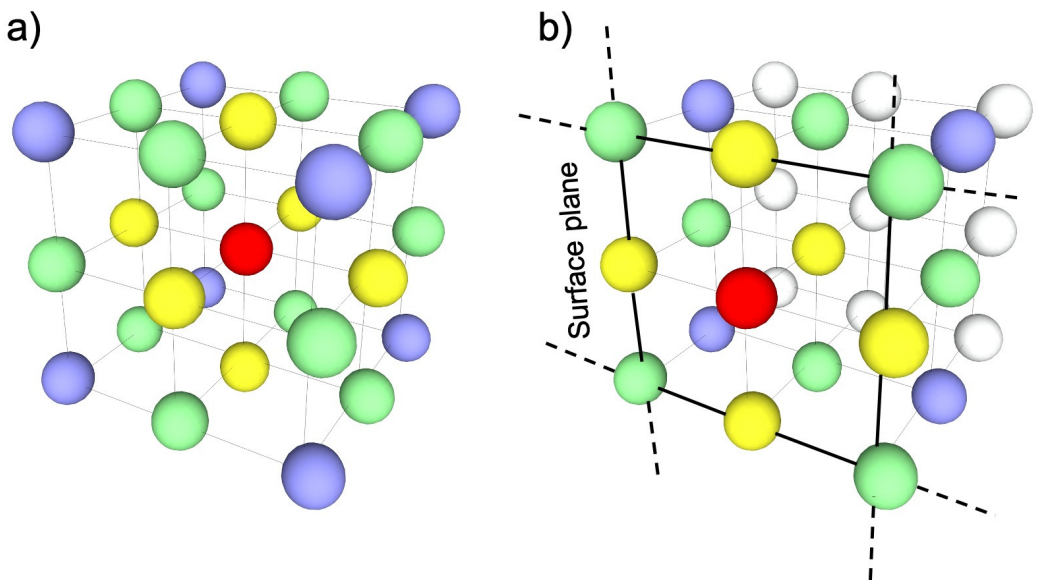

Figure 2. First, second, third neighbours (spheres in yellow, green, violet) of a reference particle (in red) placed either in the cluster's core (panel *a*) or on one of the cube's faces (panel *b*). The overall number of active neighbours on the face is always smaller than the one in the core.

and at the cluster's surface (this term grouping all layers interested by any reduction of the number of active neighbours), so that the kinetics of redistribution of the population between the two energy wells is different from core to surface. The overall cluster's contribution is therefore obtained by doing the weighted sum of the results obtained for all types of surface and core particles, the weights being given by the ratios between the number of particles of each type divided by the total number of particles in the cluster: as an example, when the surface is comprised of the first two outer layers of a cube of size $L = Nd$ made of $(N+1)^3$ particles there are $(N-3)^3$ particles in the core and 8 particles on the outer vertexes, so that the weight of the contribution from core particles is $(N-3)^3/(N+1)^3$, whilst the one from the outer vertex particles is $8/(N+1)^3$, and so on for all particles belonging in the two outer layers.

3. Results and Discussion

Room-temperature magnetic hysteresis loops of particle clusters are computed by numerically solving the rate equations [44] under a harmonic magnetic-field waveform of frequency $f = 100$ kHz with vertex field $H_V = 7.958$ kA/m (=100 Oe). It should be stressed that the considered loops are *minor* loops. In actual applications of magnetic particles for hyperthermia in living bodies it is strictly required that the vertex field be kept as low as possible, so that minor hysteresis loops are typically generated [60].

The volume fraction of magnetite nanoparticles dispersed in the host medium is

$f_V = 0.01$, a value corresponding to a rather small amount of magnetically active material when particles are homogeneously dispersed; notice that this value remains the same on the average even in the presence of clustering, although within a cluster the local volume fraction is much higher. All parameter values closely correspond to the ones typically found in *in vitro* and *in-vivo* applications of magnetic hyperthermia [10].

3.1. Clusters of monodisperse particles

Examples of the effect of particle clustering on the shape of the high-frequency hysteresis loops with vertex field $H_V = 7.958$ kA/m (100 Oe) are shown in Figure 3 for monodisperse magnetite particles of three different diameters (note that the dipolar energy term E_D increases with increasing D as $\mu^2 \sim D^6$). The cluster size is equal to $N = 10$ interparticle distances, so that each cluster contains $(N+1)^3 \simeq 1.33 \times 10^3$ particles.

Figure 3 shows that particle clustering strongly modifies the hysteresis loop's area A_L and consequently the heating efficiency of the nanoparticle assembly. In magnetic hyperthermia, a typical figure of merit is the Specific Loss Power (or SLP) defined as the power released by the nanoparticles divided by their total mass [10]. The Specific Loss Power (W_{SLP}) is directly proportional to the loop's area A_L measured at a given frequency f according to the relation $W_{SLP} = f_V A_L f/\rho_{Fe_3O_4}$ [10] where $\rho_{Fe_3O_4} \simeq 5240$ Kg/m^3 is the mass density of magnetite.

The behaviour of the loops of Figure 3 is explained taking into account the complex effects of dipolar interaction on the width of hysteresis loops, which were clarified elsewhere [45]. In brief, the widest hysteresis loop is expected - for a given frequency f and vertex field H_V - when the typical time of jump across the energy barrier (τ) is roughly equal to the driving field period $1/f$. At constant temperature, the value of τ is determined by the particle diameter, D, and by the strength of dipolar interaction (which monotonically increases with decreasing cluster size L), so that a very wide hysteresis loop emerges for one (and only one) pair of values of D and L, which makes the height of the energy barrier such that the condition $\tau \simeq 1/f$ is fulfilled. The three cases shown in Figure 3 are discussed in more detail in the following paragraphs.

When $D = 10$ nm, the interparticle distance for the homogeneous particle dispersion is $d_0 = (V/f_V)^{1/3} \simeq 37.4$ nm. At the operating frequency, the hysteresis loops are observed to be extremely narrow for both the homogeneous dispersion and all cluster sizes; in fact, for large interparticle distances the magnetization is nearly anhysteretic (left panel, red and green line); the dipolar interaction, which increases with decreasing L as $E_D \sim d^{-3} \sim L^{-3}$, is always very small and begins to play a barely discernible role for the smallest studied cluster size only ($L \simeq N d_{min} \simeq 1.2ND$), resulting in a narrow closed loop (black line). In this case, the condition $\tau \simeq 1/f$ is never fulfilled in the range of validity of the model.

When $D = 13$ nm, $d_0 = (V/f_V)^{1/3} \simeq 48.6$ nm. In this case, the SLP is initially strongly

enhanced by particle clustering (compare green and red lines in centre panel): dipolar interaction, strengthened by the reduction of the interparticle distance, increases both the coercive field and the magnetic remanence of the loops, making them much wider than the ones found in the homogeneous dispersion or in very large clusters. However, further reducing the cluster size (and the associated interparticle distance) a sharp reduction of W_{SLP} (black line) is observed. Therefore, a maximum of the SLP exists for an intermediate cluster size, where the condition $\tau \simeq 1/f$ is fulfilled.

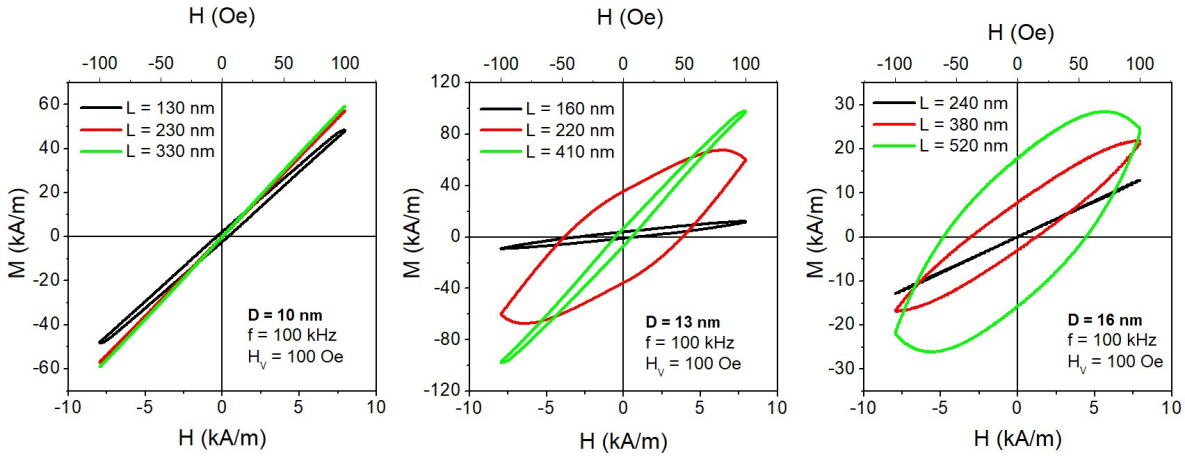

Figure 3. Minor hysteresis loops of magnetite particle clusters computed at $f = 100$ kHz for three values of the cluster size L. Left: particle diameter $D = 10$ nm; center: $D = 13$ nm; right: $D = 16$ nm. Vertex field $H_V = 7.958$ kA/m (100 Oe) in all cases.

When $D = 16$ nm, the homogeneous interparticle distance is $d_0 \simeq 59.9$ nm. In the homogeneous sample the SLP is large and monotonically decreases with decreasing cluster size. In this case, the condition $\tau \simeq 1/f$ is fulfilled for the homogeneous system only.

Therefore, particle size plays an importantl role on the effects on W_{SLP} arising from clustering. An example of the complete behaviour of the SLP as a function of cluster size over the entire interval of validity of the model is reported in the left panel of Figure 4 for $D = 13$ nm and for clusters characterized by $N = 10$ and 20 (black/red symbols, respectively). The SLP values of homogeneously dispersed and non-interacting particles are also shown (dark green symbol at right bottom, and dashed horizontal line, respectively). For the considered value of f_V the effect of dipolar interactions in the homogeneous dispersion is small and produces a modest increase in the heating efficiency with respect to the non-interacting case; however, when particle clusters begin to be formed, the heating efficiency is enhanced, reaching a value almost seven times higher than in the homogeneous system. Finally, when the cluster size becomes so small that d approaches d_{min}, W_{SLP} begins to decrease by effect of the increase in dipolar energy which takes place at small interparticle distance. Figure 4 indicates that the parameter

most affecting the $W_{SLP}(L)$ curve for particles of diameter D is the interparticle distance in a cluster, d, rather than cluster size. However, a lesser role is also played by the number of particles comprised in a cluster, because of the edge effects related to the smaller dipolar interaction existing at the cluster's surfaces. Edge effects play a greater role for small N and are responsible for the difference between the two curves shown in the left panel of Figure 4; the behaviour of additional W_{SLP} curves for $10 \leq N \leq 100$ is reported in the Supplementary Material, Section 5. The distinctive features of the W_{SLP} curves (e.g., maximum value of W_{SLP}, position of the maximum, width of the peak) are markedly influenced by the particle diameter, as also shown in the Supplementary Material. This is related to the fact that a change of D modifies the dipolar energy contribution as D^2 for any value of the interparticle distance d.

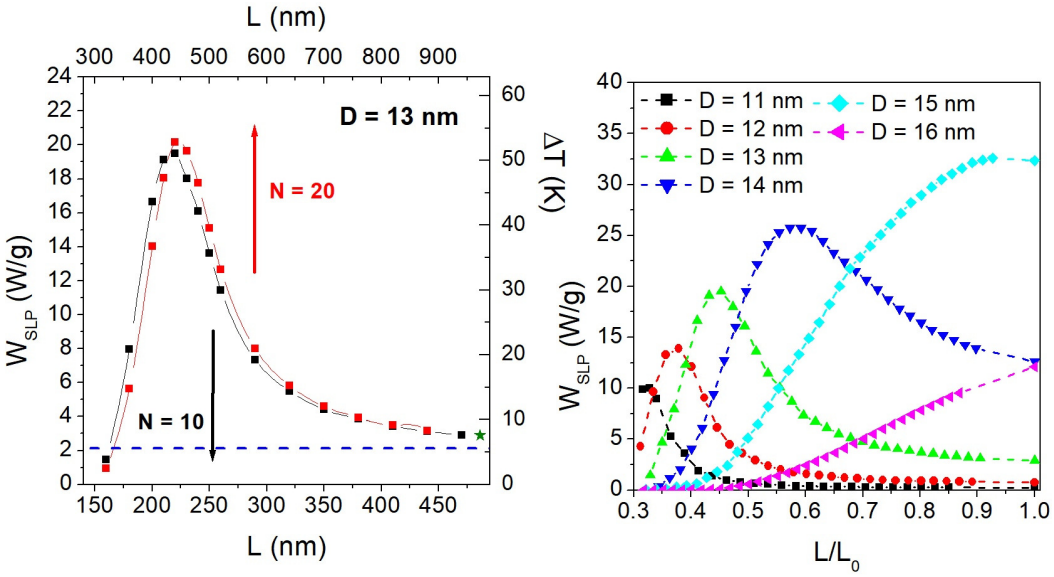

Figure 4. Left panel: behaviour of the specific loss power W_{SLP} as a function of the cluster size for two different clusters of 13-nm magnetite nanoparticles with ($N = 10$ and $N = 20$). Shown at bottom right is the value for the homogeneous distribution. The temperature increments shown on the right vertical axis have been estimated using a simple model of heating (see Section 3.4). Right panel: effect of particle clustering on W_{SLP} as a function of the reduced cluster size L/L_0 for different particle diameters (the points at $L/L_0 = 1$ are the W_{SLP} values of the homogeneous distributions; the dotted lines are guides for the eye).

The right panel of Figure 4 shows the role of particle size on the variation of the SLP by effect of particle clustering (with $N = 10$). In order to compare datasets arising from different values of D the reduced cluster size L/L_0 is used (remember that $L_0 = Nd_0 = N(V/f_V)^{1/3}$). The points at L/L_0=1 correspond to the values obtained for homogeneously dispersed particles. It should be remarked that for $D \lesssim 10$ nm the magnetization curves are basically anhysteretic not only for the homogeneous dispersion

but also for all explored cluster sizes, so that the W_{SLP} is basically zero throughout.

For the considered L/L_0 values, corresponding to the region where the model can be applied, W_{SLP} steadily decreases with decreasing cluster size when $D \geq 16$ nm. In the interval $12 \leq D \leq 15$ nm the SLP first increases with decreasing L/L_0 and is reduced when the reduced cluster size becomes small. When $D < 12$ nm, W_{SLP} steadily increases with decreasing cluster size. Such a behaviour is clearly related to dipole-dipole interaction, as discussed in Section 2.1. Generally speaking, particle clustering results in an enhanced thermal efficiency of small particles packed in dense clusters, whilst the opposite is true for large particles. The change takes place gradually with increasing D.

3.2. Cluster size maximizing the SLP

The effects described in the previous Section can be quantitatively described taking into account the ratio between the Néel relaxation time, i.e., the mean time between two flips of the magnetization across the barrier, to the driving field's period. The behaviour of W_{SLP} with the volume fraction of homogeneously dispersed particles was discussed elsewhere [45]. There, taking into account the relation between f_V and the interparticle distance d, it was shown that the curve $W_{SLP}(f_V)$ displays a single maximum corresponding to an interparticle distance such that the typical relaxation time τ is of the order of the period of the driving field, $1/f$.

In the present case, although the overall volume fraction is always the same, the interparticle distance d depends on the size of the clusters. The value of d corresponding to the maximum of W_{SLP} is found by imposing the standard condition $\tau = \tau_0\, exp\left[\frac{E_B(d)}{k_B T}\right] \simeq 1/f$ [47] where $\tau_0 \sim 10^{-9}$ s is the reciprocal of the attempt frequency and E_B is the height of the energy barrier at $H = 0$, which is a function of f_V and therefore of d through the dipolar energy term (see Equation 3). The cluster size $L^{(Max)}$ where W_{SLP} takes the maximum value turns out to be:

$$L^{(Max)} = N d^{(Max)} = \frac{N}{2}\left\{\frac{\alpha M_s^2 \pi}{18\Big[k_B T ln(1/\tau_0 f) - (\pi/6) K_u D^3\Big]}\right\}^{1/3} D^2. \qquad (6)$$

This equation is valid only for values of D such that the denominator of the expression in braces is positive. When the denominator goes to zero, the optimal interparticle distance $d^{(Max)}$ diverges, which in the model's language means that W_{SLP} would be largest for an infinitely dilute, non-interacting system (the dipolar interaction disappears in the limit of an infinite interparticle distance).

The behaviour of $L^{(Max)}$ as a function of particle diameter D is shown in the left panel of Figure 5. The two shaded regions indicate the zones where Equation 6 cannot be applied. In fact, the lower region is bounded by the $L = N d_{min} \simeq 1.2ND$ line (see Equation 5) whereas the upper region is bounded by the $L = L_0 \equiv N d_0$ line, corresponding to the homogeneous dispersion of particles.

In Figure 5, the red curve merges with the $L = 1.2ND$ line for $D \lesssim 11$ nm: in this case, $d^{(Max)} = d_{min}$, because the real absolute maximum of the $W_{SLP}(L)$ curve would

occur at a distance $d < 1.2\,D$, where the model is no longer applicable. In this interval of particle sizes, the $W_{SLP}(L)$ curve monotonically increases with decreasing L.

On the other hand, the red curve merges with the $L = L_0$ line for $D \gtrsim 15$ nm: for large particle sizes the SLP is largest for the homogeneous dispersion, and clustering reduces the heating ability of nanoparticles. Only in the interval $11 \lesssim D \lesssim 15$ nm there exists an intermediate distance $d^{(Max)}$ and an associated cluster size $L^{(Max)} = Nd^{(max)}$ where the $W_{SLP}(L)$ curve displays an absolute maximum.

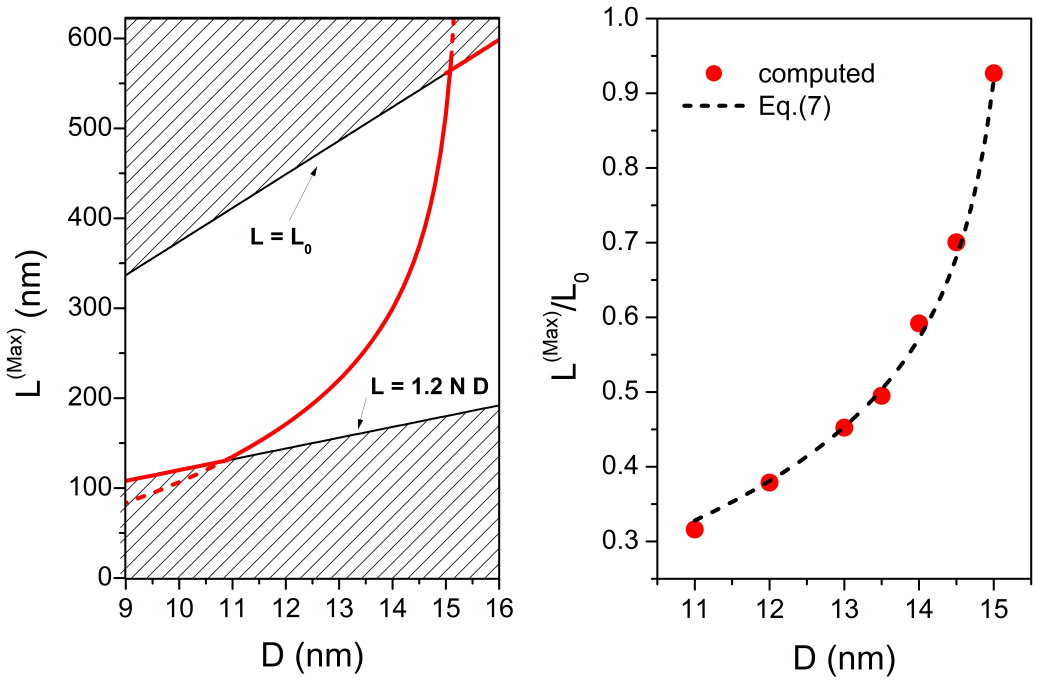

Figure 5. Left: Optimal cluster size $L^{(Max)}$ corresponding to the maximum SLP as a function of particle size D, according to Equation 6 (red line). Patterned areas: regions where the analytic expression cannot be applied (see text). Right: comparison between the values of the ratio $L^{(Max)}/L_0 \equiv d^{(Max)}/d_0$ predicted by Equation 7 and observed in the computed $W_{SLP}(L)$ curves.

The ability of Equation 6 to actually predict the position of the maximum SLP can be checked by dividing the expression for $L^{(Max)}$ by $L_0 = Nd_0 = N(\pi/6f_V)^{1/3}D$:

$$\frac{L^{(Max)}}{L_0} = \frac{d^{(Max)}}{d_0} = \frac{1}{2}\left\{\frac{\alpha M_s^2 f_V}{3\left[k_B T ln(1/\tau_0 f) - (\pi/6)K_u D^3\right]}\right\}^{1/3} D. \qquad (7)$$

The behaviour of $L^{(Max)}/L_0 = d^{(Max)}/d_0$ with diameter D is shown on the right panel of Figure 5 (black dashed line) and the actual maxima of the W_{SLP} curves simulated in the same interval of D values (including the ones shown in the right panel of Figure 5) are plotted as red circles. The agreement between the analytic expression and the results of numerical computation is very good, indicating that the application of the

model gives self-consistent results.

3.3. Particle size and maximum possible enhancement/reduction of the SLP

The effect of particle size on the maximum possible enhancement of the SLP by particle clustering is depicted in Figure 6 (black open symbols in the left panel). By "maximum possible enhancement" it is meant here that there exist one size of the clusters, $L^{(Max)}$, for which the SLP takes the highest possible value $W_{SLP}^{(Max)}$ for a given particle size.

As previously discussed, an absolute maximum of the $W_{SLP}(L)$ curve is found for particle sizes larger than $D = 11$ nm only; therefore, this region is shown in Figure 6. The red circles represent the W_{SLP} values obtained for homogeneously dispersed particles. When D is decreased from $D = 18$ nm to 11 nm, $W_{SLP}^{(Hom)}$ increases, reaches a maximum for D close to 15 nm, then decreases and becomes rapidly negligible. Such a behaviour has been explained in detail elsewhere [45] and was briefly discussed in Section 3.1. A sharp maximum of $W_{SLP}^{(Hom)}$ is found when the hysteresis loop is very wide; in turn, the loop is widest when the typical time of jump across the energy barrier (τ) becomes roughly equal to the driving field period $1/f$ (the condition is verified, for a homogeneous system, when $D \simeq 15$ nm).
On the contrary, the open symbols represent the $W_{SLP}^{(Max)}$ values predicted in clustered systems. It is observed that for $D \gtrsim 15$ nm the two datasets are perfectly coincident: this means that particle clustering does not give a better SLP than the one of the homogeneous dispersion (actually, clustering decreases the SLP in this region). Below 15 nm, however, the values of $W_{SLP}^{(Max)}$, although decreasing with decreasing D, remain significanty higher than the ones of $W_{SLP}^{(Hom)}$. This means that in this region the formation of clusters of suitable size permits to effectively enhance the heating ability of nanoparticles.

No exact analytic expression of $W_{SLP}^{(Max)}$ can be derived from the rate equations; however, its functional dependence on particle size D can be determined by exploiting the condition $\tau \simeq 1/f$, as discussed in the Supplementary Material, Section 6. In particular, in the interval of validity of Eq.6 the functional dependence of the maximum SLP on D turns out to be of the type:

$$W_{SLP}^{(Max)}(D) = \frac{a}{1 + exp(-\beta D^3)} - c \tag{8}$$

Meaning and values of the constants $a, \beta, c \simeq a/2$ are discussed in the Supplementary Material. The values of $W_{SLP}^{(Max)}$ obtained from the numerical solution of the rate equations are well fitted by Eq. 8 (dashed blue line in Figure 6) with the following parameter values: $a = 191.90$ W/g, $\beta = 2.55 \times 10^{17}$ cm^{-3}, $c = 102.38$ W/g. It should be noted that while the calculation done in the Supplementary Material does not permit to obtain the values of constants a and c which are adjustable parameters derived from the fit, the quantity β, instrumental in determining the functional dependence of $W_{SLP}^{(max)}$ on

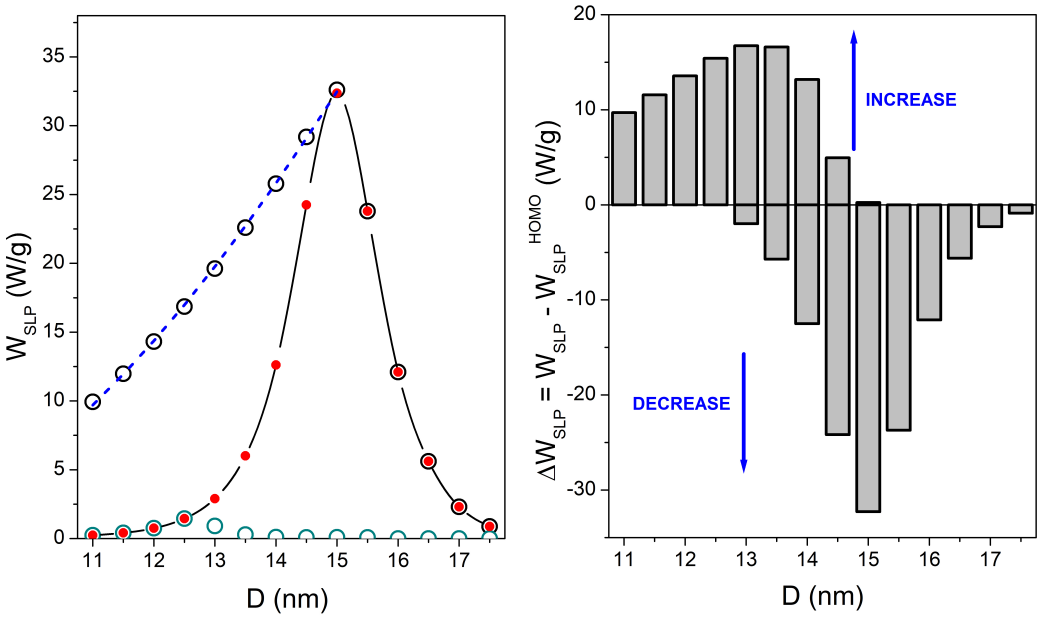

Figure 6. Left panel: red circles: SLP as a function of particle size in the interval 11 $\leq D \leq$ 16 nm for homogeneously distributed particles; black open circles: maximum possible SLP for clustered particles in the same range; dashed blue line: fit to Eq. 8; green open circles: minimum possible SLP for clustered particles. Right panel: tunability of the SLP as a function of particle diameter D; ΔW_{SLP} is the difference between the SLP of clustered and homogeneously distributed particles.

D, is accurately predicted by the calculation.

On the other hand, in view of diagnostic applications such as MPI, it may be interesting to study under which conditions the more effective *reduction* of the SLP on clustering is to be expected. The results are also shown in the left panel of Figure 6 (green open symbols). For low particle sizes ($D \leq 12.5$ nm) the minimum possible value of the SLP ($W_{SLP}^{(Min)}$) corresponds to the homogeneous dispersion of particles; for higher D values particle clustering brings about a substantial reduction of the SLP with respect to the homogeneous case, so that $W_{SLP}^{(Min)}$ becomes very close to zero.

A suitable graphical representation of the SLP modulation by effect of particle clustering is shown in the right panel of Figure 6. The quantity $\Delta W_{SLP} = W_{SLP} - W_{SLP}^{(Hom)}$ measures the positive and/or negative variation of the SLP produced by clustered particles with respect to the homogeneous case, which is taken as a baseline. The parameter ΔW_{SLP} helps clarify the different behaviour of particles in dependence of their size: small particles ($D \leq 12.5$ nm) can only increase their SLP on clustering, whereas cluster formation can only reduce the SLP of large particles ($D \gtrsim 15$ nm). For intermediate values of D (in the present case, around 14 nm) clustering of particles may either en-

hance or reduce the SLP with respect to the homogeneous case, depending on the size of clusters. From this viewpoint, this is the particle size which ensures the best tunability of the SLP.

The model's features can be discussed along with the ones of recent approaches to the properties of compact particle clusters, based either on numerical solutions of the LLG equation [42, 61, 62, 63] or Monte-Carlo simulations [43, 64, 65, 66].

In some simulations the effects of interactions inside the clusters are not considered in detail [67, 68]. In other papers, a strictly linear approach is adopted to describe magnetization processes leading to the production of energy by clustered particles [68, 69, 70]). In all cases the simulations are necessarily aimed to describe very small clusters, the number of individual particles per cluster never exceeding one hundred, and often being significantly lesser. In principle, the present method poses no limits to the size of clusters, takes into account the interactions inside clusters in an effective way, and is able to provide reliable results even in the operating conditions of therapeutic hyperthermia where the linear model is no longer applicable, resulting in an imprecise temperature estimate [47].

Some recent numerical results appear to be either not entirely explained (e.g., the maximum of the SLP for a specific interparticle distance in a cluster [61]) or contradictory (e.g., the contrasting conclusions that SLP is not affected by particle clustering [64, 63] and that in isotropic clusters it is lower than in individual particles [42, 43], whereas some measurements do show an increase of SLP on clustering [33, 41]). These issues can be coherently explained by the present approach, which is based on an accurate representation of particle magnetization and is remarkably flexible, in the sense that the relevant physical parameters can be modulated more freely than in strictly numerical methods.

3.4. Particle clustering and temperature increment

The temperature increment measured during the heating process of a diamagnetic host medium is modified by nanoparticle clustering as a consequence of the effects on the SLP we have just described. Specific features of magnetic hyperthermia achieved using either non-interacting or interacting particles have been discussed in detail elsewhere [45, 47]. Here, an approximate estimate of the temperature achieved by a sample containing a fraction $f_V = 0.01$ of magnetite nanoparticles, either evenly dispersed or forming clusters, is done using the simple approach outlined in the Supplementary Material, Section 7, where the time- and space-dependent temperature increment resulting by excitation of clustered particles is discussed. A typical result is reported on the right vertical axis of Figure 4, left panel. It can be concluded that particle clustering can significantly improve the target temperature with respect to the homogeneous case.

Looking for the most convenient use of clusters of particles, a simple rule of thumb is given here: if magnetite particles larger than 14-15 nm are being considered for

practical application requiring a high SLP, the best strategy is to have a homogeneous dispersion in, or around, the target tissue; conversely, if the particles are in the 11-14 size range, particle clustering offers a definitely advantageous way to increase the heating performance without the need of using a large amount of inoculated metal ions.

As a matter of fact, many different sizes of iron oxide nanoparticles have been considered for practical, i.e., *in-vivo* applications of magnetic hyperthermia [7]. On the basis of physiology considerations, particle diameters between 12 and 50 nm have been indicated as ideal for application in biomedicine, the lower limit being dictated by the requirement that the particles should be large enough so that they do not cross the pores of a blood vessel wall, which are typically smaller than 12 nm [71]. The upper limit is instead defined with reference to the ease of transport in the blood circulation [71]. Let us stress, however, that magnetite particles larger than 18-20 nm (depending on the parameter values) are basically ineffective as heaters of a living tissue when submitted to a radio-frequency magnetic field whose amplitude is sufficiently small to be tolerated by patients [10].

Magnetic fluid hyperthermia has been demonstrated and used in actual clinical trials using 12-13 nm magnetite nanoparticles with a bio-compatible coating (NanoTherm (R), [72]). However, in this case the solution is usually inoculated at a high concentration of 112 mg/mL of iron [72], corresponding to a magnetite particle volume fraction $f_V \simeq 0.03$, because a large local amount of magnetite is needed to achieve thermal tissue ablation. When small particles are to be used, particle clusters of suitable size can provide a superior heating efficiency, allowing one to significantly reduce the amount of particle concentration in the magnetic fluid and avoid the detrimental consequences of the inoculation of a high volume fraction of nanoparticles in a living body.

On the other hand, use of magnetite nanoparticles in MPI of both healthy and diseased tissues [5] may imply applying frequencies and amplitudes of the magnetic field such that local heating of the tissue - which is an undesired by-product of the technique in this case - cannot be disregarded [16]. In the light of the present analysis, such a by-product could be avoided by dispersing compact clusters of large ($D > 15$ nm) particles in the tissue, instead of using single particles. In this case the magnetic interactions within clusters located at the field-free point (or line) of the MPI scanner [5] will substantially reduce the hysteresis loops' area keeping the released heat low, while the signal generated by the switching cluster magnetization and exploited to produce the tomographic image is expected to remain easily detectable by a typical MPI setup.

3.5. Clusters of polydisperse particles

Particle clustering has been shown to significantly change the SLP of monodisperse nanoparticles. However, the effect of clustering is so dependent on particle diameter that one can ask whether in polydisperse systems a modulation of thermal efficiency is still possible. Only the case of SLP enhancement is considered here. We have

explored the variation of W_{SLP} for clustering particles distributed in size according to a gaussian distribution function $p(D)$ (some examples are shown in the right panel of Figure 7). Particles of different diameter are assumed to randomly occupy the sites on the simple cubic lattice representing the homogeneous particle distribution. The average interparticle distance is now $\overline{d_0} = \overline{V}/f_V$ where $\overline{V}$ is the average particle volume. The energy barrier of each particle is modified by the expression of E_D given in Equation 4.

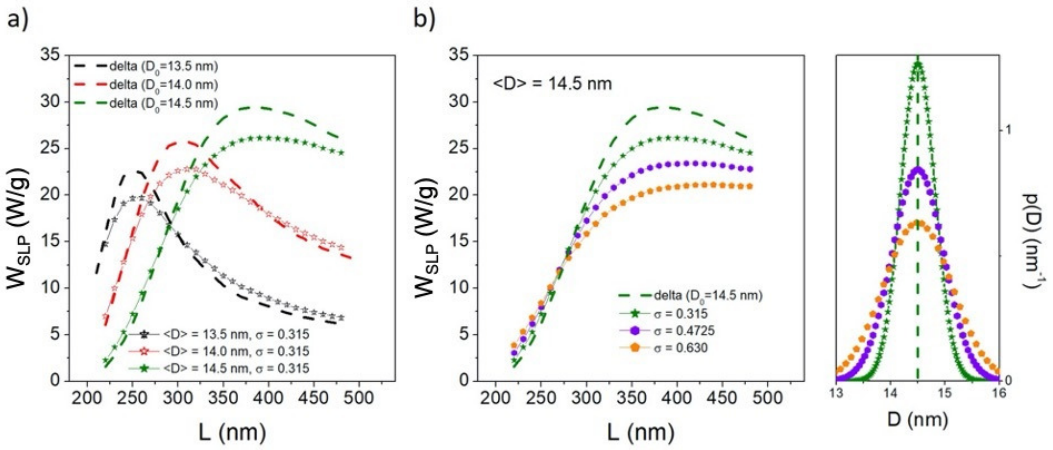

Figure 7. Panel a): effect of a narrow Gaussian distribution of magnetite particle sizes around three values of D on the behaviour of the SLP with the size of clusters (for $N = 10$); the dashed lines apply to the corresponding monodisperse systems. Panel b): smoothing effect of an increasing standard deviation of the Gaussian distribution centred at $D = 14.5$ nm. The Gaussian functions used in panels a) and b) are shown in the rightmost panel.

The results are reported in Figure 7. The effect of a narrow gaussian distribution with standard deviation $\sigma = 0.315$ nm centred at three different values of D is shown in panel a along with the curves obtained in the corresponding monodisperse particles (dashed lines). Therefore, a narrow $p(D)$ function preserves the main features of the enhancement of the W_{SLP} parameter induced by particle clustering. It should be noted that the present value of σ corresponds to a range of particle sizes in the 13.5 -15.5 nm interval (see green curve in the right panel), i.e., a range of about 2 nm which is compatible with the requirements for hyperthermia-based therapy [7, 72], where however the conceptual aim is to deal with an even narrower dispersion of particle sizes. An example of the smoothing effect observed by increasing the standard deviation of $p(D)$ is shown in panel b of Figure 7, where the $W_{SLP}(d)$ curves corresponding to the delta function and to three gaussian distributions, all peaked at $D = 14.5$ nm, are reported. The colours correspond to the σ values reported in the centre panel. Of course, the larger σ, the smoother and featureless is the $W_{SLP}(d)$ curve. Generally speaking, beneficial effects of particle clustering on thermal efficiency clearly emerge when the particle distribution function is sufficiently narrow.

4. Conclusion

The formation of dense clusters of magnetite nanoparticles significantly modifies their heating efficiency with respect to the homogeneous dispersion. The effect is dominated by dipole-dipole interaction which can become particularly strong inside a cluster because of the lower mean interparticle distance. This results in an increase of the energy barrier which has to be overcome by the magnetization of a particle.

A simple idealized model of magnetic clusters has been developed. The effect of intra-cluster dipolar interactions on the shape of minor hysteresis loops turns out to be critically dependent on particle size. As a consequence, clustering of small magnetite nanoparticles ($D \lesssim 14$ nm) leads to a significant enhancement of the specific loss power, and clustering of large particles ($D \gtrsim 15$ nm) reduces their ability to heat. In other words, large particles are more efficient as heaters when they are homogeneously distributed in a host medium, whereas dense clusters comprised of small particles have a definitely higher SLP than the corresponding homogeneous dispersions. This circumstance can be exploited to produce suitable nanoparticle preparations intended either to enhance the thermal efficiency of magnetic particles (a property sought after in such distant application areas as magnetic hyperthermia for anti-cancer therapy and flow assurance in oil production and transport), or to reduce the undesired heating of tissues as in Magnetic Particle Imaging.

The particle size ensuring the best modulation ability of the SLP is $D \approx 14$ nm: in this case, the formation of clusters of proper size can either increase or decrease the SLP, which would permit to prepare multi-purpose nanomaterials (e.g., ferrofluids) tailored for specific applications.

In polydisperse systems, the contrasting effects of dipolar interactions in particles of different size tend to counterbalance, therefore reducing the effect of particle clustering on the SLP. However, narrow size distributions as the ones used in magnetic hyperthermia still retain most of the features observed in monodisperse particle systems.

This model permits to freely modify all parameters playing a role in the process of cyclic magnetization, so that one can easily interpret the magnetic behaviour of a nanoparticle system and draw a comprehensive, self consistent picture of the resulting effects with a predictive character that may escape other approaches.

In conclusion, dipole-dipole interaction among particles is particularly sensitive to the degree of uniformity of the particle distribution in a host material or a tissue. This property can be used in a variety of applications by creating compact clusters where the individual particles are physically kept separated from each other, e.g., by a diamagnetic coating. Clusters of this type are characterized by a very different magnetic behaviour and efficiency in the release of thermal energy with respect to homogeneous dispersions. The volume of real compact particle clusters (comprised of $\sim 10^3 \div 10^5$ individual particles) is much smaller than the one of a typical target in a living body (of the order of the cubic centimeter), so that each cluster can still be safely considered to be a "point-

like" heat source on the macroscopic scale; in the case of clustering, a non-homogeneous distribution of heat on the nanometer scale is expected; however, heat is transferred in a living body non only by thermal diffusion but also, and more efficiently, by convection through the blood flow, so that a uniform temperature is expected to be quickly achieved everywhere in the target volume even in the presence of a non-homogeneous distribution of individual particles.

The effects studied in the present paper should be properly taken into account in the efforts towards the optimization of all applications involving high-frequency magnetization processes of magnetic particles.

References

[1] Thanh N T K 2018 *Clinical Applications of Magnetic Nanoparticles: From Fabrication to Clinical Applications* ed N T K Thanh (CRC Press)

[2] Zhou K, Zhou X, Liu J and Huang Z 2020 Application of magnetic nanoparticles in petroleum industry: A review *J. Pet. Sci. Eng.* **188** 106943

[3] Haseeb Q, Hamdani S D A, Akram A, Khan D A, Rajput T A and Babar M M 2020 *Nanobiotechnology: Paving the Way to Personalized Medicine NanoBioMedicine* (Springer Singapore) pp 17–32

[4] Périgo E A, Hemery G, Sandre O, Ortega D, Garaio E, Plazaola F and Teran F J 2015 Fundamentals and advances in magnetic hyperthermia *Appl. Phys. Rev.* **2** 1–35

[5] Bakenecker A, Ahlborg M, Debbeler C, Kaethner C and Lüdtke-Buzug K 2018 *Magnetic Particle Imaging Precision Medicine: Tools and Quantitative Approaches* (Elsevier Inc.) pp 183–228

[6] Sengul A B and Asmatulu E 2020 Toxicity of metal and metal oxide nanoparticles: a review *Environ. Chem. Lett.* **18** 1659–83

[7] Beola L, Gutiérrez L, Grazú V and Asín L 2019 A Roadmap to the Standardization of In Vivo Magnetic Hyperthermia *Nanomaterials for Magnetic and Optical Hyperthermia Applications* ed R M Fratila and J M De La Fuente (Elsevier Ltd) pp 317–37

[8] Allia P, Barrera G and Tiberto P 2019 Nonharmonic Driving Fields for Enhancement of Nanoparticle Heating Efficiency in Magnetic Hyperthermia *Phys. Rev. Appl.* **12** 034041

[9] Barrera G, Allia P and Tiberto P 2020 Fine tuning and optimization of magnetic hyperthermia treatments using versatile trapezoidal driving-field waveforms *Nanoscale Adv.* **2** 4652-4664

[10] Dutz S and Hergt R 2013 Magnetic nanoparticle heating and heat transfer on a microscale: Basic principles, realities and physical limitations of hyperthermia for tumour therapy *Int. J. Hyperth.* **29** 790–800

[11] Negut I and Grumezescu V 2019 *Nanoparticles and hyperthermia* (Elsevier Inc.)

[12] Marino A, Camponovo A, Degl'Innocenti A, Bartolucci M, Tapeinos C, Martinelli C, De Pasquale D, Santoro F, Mollo V, Arai S, Suzuki M, Harada Y, Petretto A and Ciofani G 2019 Multifunctional temozolomide-loaded lipid superparamagnetic nanovectors: Dual targeting and disintegration of glioblastoma spheroids by synergic chemotherapy and hyperthermia treatment *Nanoscale* **11** 21227–48

[13] Ding J, Chen J, Gao L, Jiang Z, Zhang Y, Li M, Xiao Q, Lee S S and Chen X 2019 Engineered nanomedicines with enhanced tumor penetration *Nano Today* **29** 100800

[14] Talebloo N, Gudi M, Robertson N and Wang P 2020 Magnetic Particle Imaging: Current Applications in Biomedical Research *J. Magn. Reson. Imaging* **51** 1659–68

[15] Knopp T, Gdaniec N and Möddel M 2017 Magnetic particle imaging: From proof of principle to preclinical applications *Phys. Med. Biol.* **62** R124–78

[16] Wells J, Paysen H, Kosch O and Wiekhorst F 2020 Heat dissipation and safety considerations during lissajous scanning magnetic particle imaging *Int. J. Magn. Part. Imaging* **6** 1–3

[17] Chen H, Kaminski M D, Liu X, Mertz C J, Xie Y, Torno M D and Rosengart A J 2007 A novel human detoxification system based on nanoscale bioengineering and magnetic separation techniques *Med. Hypoth.* **68** 1071–1079

[18] Chen H, Ebner A D, Ritter J A, Kaminsku M D and Rosengart A J 2008 Theoretical Analysis of a Magnetic Separator Device for Ex-Vivo Blood Detoxification *Separ. Sci. Technol.* **43** 996-1020

[19] Stamopoulos D, Bouziotis P, Benaki D, Kotsovassilis C and Zirogiannis P N 2008 Utilization of nanobiotechnology in haemodialysis: mock-dialysis experiments on homocysteine *Nephrol. Dial. Transplant.* **23** 3234-3239

[20] Stamopoulos D, Manios E, Gogola V, Benaki D, Bouziotis P, Niarchos D and Pissas M 2008 Bare and protein-conjugated Fe_3O_4 ferromagnetic nanoparticles for utilization in magnetically assisted hemodialysis: biocompatibility with human blood cells *Nanotechnology* **51** 505101

[21] Stamopoulos D, Gogola V, Manios E, Gourni E, Benaki D, Niarchos D and Pissas M 2009 Biocompatibility and Solubility of Fe_3O_4-BSA Conjugates with Human Blood *Curr. Nanosci.* **5** 177-181

[22] Moersdorf D, Hugounenq P, Phuoc L T, Mamlouk-Chaouachi H, Felder-Flesch D, Begin-Colin S, Pourroy G and Bernhardt I 2010 *Adv. Biosci. Biotechnol.* **1** 439-443

[23] Rodrigues R O, Bañobre-López M, Juan Gallo J, Tavares P B, Silva A M T, Lima R and Gomes H T 2016 Haemocompatibility of iron oxide nanoparticles synthesized for theranostic applications: a high-sensitivity microfluidic tool *J. Nanopart. Res.* **18** 194

[24] Nosrati H, Salehiabar M, Fridoni M, Abdollahifar M A, Manjili H K, Davaran S and Danafar H 2019 New Insight about Biocompatibility and Biodegradability of Iron Oxide Magnetic Nanoparticles: Stereological and In Vivo MRI Monitor *Sci. Reports* **9** 7173

[25] Karageorgou M A, Bouziotis P, Vranješ-Djurić S and Stamopoulos D 2020 Hemocompatibility of gallium-68 labeled iron oxide nanoparticles coated with 2,3-dicarboxypropane-1,1-diphosphonic acid *Mat. Sci. Eng. C* **115** 111121

[26] Shingala J, Shah V, Dudhat K and Shah M 2020 Evolution of nanomaterials in petroleum industries: application and the challenges *J. Pet. Explor. Prod. Technol.* **10** 3993–4006

[27] Rosenweig R E 2002 Heating magnetic fluid with alternating magnetic fiel *J. Magn. Magn. Mater.* **252** 370–2

[28] Lahiri B B, Ranoo S and Philip J 2017 Uncertainties in the estimation of specific absorption rate during radiofrequency alternating magnetic field induced non-adiabatic heating of ferrofluids *J. Phys. D. Appl. Phys.* **50** 455005

[29] Wildeboer R R, Southern P and Pankhurst Q A 2014 On the reliable measurement of specific absorption rates and intrinsic loss parameters in magnetic hyperthermia materials *J. Phys. D. Appl. Phys.* **47** 495003

[30] Wells J, Kazakova O, Posth O, Steinhoff U, Petronis S, Bogart L K, Southern P, Pankhurst Q and Johansson C 2017 Standardisation of magnetic nanoparticles in liquid suspension *J. Phys. D. Appl. Phys.* **50** 383003

[31] Makridis A, Curto S, Van Rhoon G C, Samaras T and Angelakeris M 2019 A standardisation protocol for accurate evaluation of specific loss power in magnetic hyperthermia *J. Phys. D. Appl. Phys.* **52** 255001

[32] Shasha C and Krishnan K M 2020 Nonequilibrium Dynamics of Magnetic Nanoparticles with Applications in Biomedicine *Adv. Mater.* **1904131** 48–50

[33] Lartigue L, Hugounenq P, Alloyeau D, Clarke S P, Lévy, Michael, Bacri J-C, Bazzi R, Brougham D F, Wilhelm C and Gazeau F 2012 Cooperative Organization in Iron Oxide Multi-Core Nanoparticles Potentiates Their Efficiency as Heating Mediators and MRI Contrast Agents *ACS Nano* **6** 10935–49

[34] Herman K, Lang M E and Pich A 2018 Tunable clustering of magnetic nanoparticles in microgels: Enhanced magnetic relaxivity by modulation of network architecture *Nanoscale* **10** 3884–92

[35] Li Y, Hu K, Chen B, Liang Y, Fan F, Sun J, Zhang Y and Gu N 2017 Fe_3O_4@PSC nanoparticle clusters with enhanced magnetic properties prepared by alternating-current magnetic field

assisted co-precipitation *Colloids Surfaces A Physicochem. Eng. Asp.* **520** 348–54
[36] Shen S, Wang S, Zheng R, Zhu X, Jiang X, Fu D and Yang W 2015 Magnetic nanoparticle clusters for photothermal therapy with near-infrared irradiation *Biomaterials* **39** 67–74
[37] Togashi T, Naka T, Asahina S, Sato K, Takami S and Adschiri T 2011 Surfactant-assisted one-pot synthesis of superparamagnetic magnetite nanoparticle clusters with tunable cluster size and magnetic field sensitivity *Dalt. Trans.* **40** 1073–8
[38] Turcu R, Socoliuc V, Craciunescu I, Petran A, Paulus A, Franzreb M, Vasile E and Vekas L 2015 Magnetic microgels, a promising candidate for enhanced magnetic adsorbent particles in bioseparation: Synthesis, physicochemical characterization, and separation performance *Soft Matter* **11** 1008–18
[39] Pearce J, Giustini A, Stigliano R and Hoopes P J 2013 Magnetic heating of nanoparticles: The importance of particle clustering to achieve therapeutic temperatures *J. Nanotechnol. Eng. Med.* **4** 0110071-01100714
[40] Roveimiab Z, Mahdavian A R, Biazar E and Heidari K S 2012 Preparation of Magnetic Chitosan Nanocomposite Particles and Their Susceptibility for Cellular Separation Applications *J. Colloid Sci. Biotechnol.* **1** 82–8
[41] Yang Qu, Jianbo Li, Jie Ren, Junzhao Leng, Chao Lin and D S 2014 Enhanced Magnetic Fluid Hyperthermia by Micellar *Magnetic Appl. Mater. Interfaces* **6** 16867–16879
[42] Usov N A, Serebryakova O N and Tarasov V P 2017 Interaction Effects in Assembly of Magnetic Nanoparticles *Nanoscale Res. Lett.* **12** 489
[43] Fu R, Yan Y, Roberts C, Liu Z and Chen Y 2018 The role of dipole interactions in hyperthermia heating colloidal clusters of densely-packed superparamagnetic nanoparticles *Sci. Rep.* **8** 1–10
[44] Allia P, Barrera G and Tiberto P 2020 Hysteresis effects in magnetic nanoparticles: A simplified rate-equation approach *J. Magn. Magn. Mater.* **496** 165927
[45] Barrera G, Allia P and Tiberto P 2021 Dipolar Interactions Among Magnetite Nanoparticles For Magnetic Hyperthermia: A Rate-Equation Approach *Nanoscale* Accepted Manuscript https://doi.org/10.1039/D0NR07397K
[46] Dormann J L, Fiorani D and Tronc E 1999 On the models for interparticle interactions in nanoparticle assemblies: comparison with experimental results *J. Magn. Magn. Mater.* **202** 251–67
[47] Barrera G, Allia P and Tiberto P 2020 Temperature-dependent heating efficiency of magnetic nanoparticles for applications in precision nanomedicine *Nanoscale* **12** 6360–77
[48] Usov N A 2011 Numerical simulation of field-cooled and zero field-cooled processes for assembly of superparamagnetic nanoparticles with uniaxial anisotropy *J. Appl. Phys.* **109** 023913
[49] Soukup D, Moise S, Céspedes E, Dobson J and Telling N D 2015 In Situ Measurement of Magnetization Relaxation of Internalized Nanoparticles in Live Cells *ACS Nano* **9** 231–40
[50] Usov N A and Serebryakova O N 2020 Equilibrium properties of assembly of interacting superparamagnetic nanoparticles *Sci. Rep.* **10** 1–14
[51] Morup S 1994 Superparamagnetism and Spin Glass Ordering in Magnetic Nanocomposites *Europhys. Lett.* **28** 671–6
[52] Moya C, Iglesias Ó, Batlle X and Labarta A 2015 Quantification of Dipolar Interactions in $Fe_{3-x}O_4$ Nanoparticles *J. Phys. Chem. C* **119** 24142–8
[53] Ruta S, Chantrell R and Hovorka O 2015 Unified model of hyperthermia via hysteresis heating in systems of interacting magnetic nanoparticles *Sci. Rep.* **5** 1–7
[54] Brown W F 1963 Thermal fluctuations of a single-domain particle *Phys. Rev.* **130** 1677–86
[55] Jeon S, Hurley K R, Bischof J C, Haynes C L and Hogan C J 2016 Quantifying intra- and extracellular aggregation of iron oxide nanoparticles and its influence on specific absorption rate *Nanoscale* **8** 16053–64
[56] Lisjak D and Mertelj A 2018 Anisotropic magnetic nanoparticles: A review of their properties, syntheses and potential applications *Prog. Mater. Sci.* **95** 286–328
[57] Fiorani D and Peddis D 2014 Understanding dynamics of interacting magnetic nanoparticles: From

the weak interaction regime to the collective superspin glass state *Journal of Physics: Conference Series vol 521 (Institute of Physics Publishing)* **521** 012006

[58] Rivas Rojas P C, Tancredi P, Moscoso Londoño O, Knobel M and Socolovsky L M 2018 Tuning dipolar magnetic interactions by controlling individual silica coating of iron oxide nanoparticles *J. Magn. Magn. Mater.* **451** 688–96

[59] Cuchillo A, Rivas-Rojas P, Tancredi P, Socolovsky L M and Vargas P 2020 Combining dipolar and anisotropic contributions to properly describe the magnetic properties of magnetic nanoparticles real systems *J. Magn. Magn. Mater.* **508** 166842

[60] Cullity B D and Graham C D 2009 *Introduction to Magnetic Materials*

[61] Anand M, Carrey J and Banerjee V 2012 Spin morphologies and heat dissipation in spherical assemblies of magnetic nanoparticles *Phys.Rev.B* **94** 094425

[62] Kuznetsov A A 2019 Zero-Field and Field-Induced Interactions between Multicore Magnetic Nanoparticles *Nanomater.* **9** 718

[63] Lattuada M 2019 Effect of Clustering on the Heat Generated by Superparamagnetic Iron Oxide Nanoparticles *Chimia* **73** 39-42

[64] Fu R, Yan Y Y and Roberts C 2015 Study of the effect of dipole interactions on hyperthermia heating the cluster composed of superparamagnetic nanoparticles *AIP Advances* **5** 127232

[65] Bender P, Wetterskog E, Honecker D, Fock J, Frandsen C, Moerland C, Bogart L K, Posth O., Szczerba W, Gavilán H, Costo R, Fernández-Díaz M T, González-Alonso D, Fernández Barquín L and Johansson C. 2018 Dipolar-coupled moment correlations in clusters of magnetic nanoparticles *Phys.Rev.* B **98** 224420

[66] Anand M 2021 Hysteresis in Two Dimensional Arrays of Magnetic Nanoparticles, arXiv:2104.02961v1 [cond-mat.mtrl-sci] 7 Apr 2021

[67] Pearce J, Giustini A, Stigliano R and Hoopes P J 2014 Magnetic Heating of Nanoparticles: The Importance of Particle Clustering to Achieve Therapeutic Temperatures *J. Nanotech. Engin. and Med.* **4** 011007

[68] Halgamuge M N and Song T 2020 Optimizing Heating Efficiency of Hyperthermia: Specific Loss Power of Magnetic Sphere Composed of Superparamagnetic Nanoparticles *Progr. Electromagn. Res. B* **87** 1-17

[69] Wang C, Hsu C H, Li Z, Hwang L P, Lin Y C, Chou P T and Lin Y Y 2017 E ffective heating of magnetic nanoparticle aggregates for in vivo nano-theranostic hyperthermia *Int. J. Nanomed.* **I2** 6273-6287

[70] Tang Y, Jin T and Flesch R C C 2017 Numerical temperature analysis of magnetic hyperthermia considering nanoparticle clustering and blood vessels Tang Y, Jin T and Flesch R C C 2017 Numerical temperature analysis of magnetic hyperthermia considering nanoparticle clustering and blood vessels *IEEE Trans. Magnetics* **53** 5400106

[71] Stylianopoulos T *Eur. J. Nanomed.* 2016 Intelligent drug delivery systems for the treatment of solid tumors *Eur. J. Nanomed.* **8** 9

[72] Maier-Hauff K, Ulrich F, Nestler D, Niehoff H, Wust P, Thiesen B, Orawa H, Budach V and Jordan A 2011 Efficacy and safety of intratumoral thermotherapy using magnetic iron-oxide nanoparticles combined with external beam radiotherapy on patients with recurrent glioblastoma multiforme *J. Neurooncol.* **103** 317–24

Heating ability modulation by clustering of magnetic particles for precision therapy and diagnosis

Gabriele Barrera, Paolo Allia and Paola Tiberto

INRIM, Advanced Materials Metrology and Life Sciences, Strada delle Cacce 91, 10135 Torino, Italy

E-mail: g.barrera@inrim.it

February 2021

Abstract. Magnetic and thermal properties of clustered magnetite nanoparticles submitted to a high-frequency magnetic field is studied by means of rate equations. A simple model of large particle clusters (containing more than one hundred individual particles) is introduced. Dipolar interactions among clustered particles markedly modifiy shape and area of the hysteresis loops in a way critically dependent on particle size and cluster dimensions, thereby modulating the power released as heat to a host medium. For monodisperse and polydisperse systems, particle clustering can lead to either a significant enhancement or a definite reduction of the released power; in particular cases the same particles can produce opposite effects in dependence of the dimensions of the clusters. Modulation by clustering of the heating ability of magnetic nanoparticles has impact on applications requiring optimization and accurate control of temperature in the host medium, such as magnetic hyperthermia for precision therapy or fluid flow management, and advanced diagnostics involving magnetic tracers.

1. Introduction

The interest towards the high-frequency properties of magnetic nanoparticles has substantially increased with the rise of applications of magnetically driven particles as sources of heat or contrast agents. Applications include such different areas as biomedicine [1] and oil extraction and transportation industry [2] where, despite the diversity of subjects, basically the same language, methods, and physical parameters are involved.

In biomedicine, the functional properties of magnetic nanoparticles play an important role in rapidly evolving techniques for precision therapy [3] and diagnosis, such as Magnetic Hyperthermia (MH) [4] where particles serve as point-like heat sources around or inside internal organs of living bodies, and Magnetic Particle Imaging (MPI) [5] where they act as magnetic tracers. In both cases, modulating in a controlled way the heating power released by particles to the surrounding tissues is mandatory in order to

achieve an efficient, non damaging therapeutic practice or visualization. In MH the aim is usually to maximize the heating ability of magnetic particles whereas in MPI, where particles serve as non-invasive, diagnostic tracers, the released power should usually be kept as low as possible.

Magnetic hyperthermia has been introduced in the clinical practice as a precision therapy aimed to inflict damage to malignant cells by means of the heat generated by nanoparticles containing transition-metal atoms or ions. The nanoparticles, which must be as biocompatible as possible [6], are submitted to a magnetic field H of high frequency (typically in the interval 10 kHz$\leq f \leq$1 Mhz) and suitable amplitude [7] with harmonic or non-harmonic time behaviour [8, 9]. Human physiology imposes limits on the physical parameters of operation; in particular, the product Hf cannot exceed an upper threshold in order to avoid discomfort or even nuisance to patients [10]. MH can be exploited either as a standalone therapy [11] or in association with other curing techniques, such as chemotherapy or radiotherapy [12]; in this case, the heat released by magnetic nanoparticles favours a higher therapeutic efficacy and a deeper malignant tissue penetration [13].

In MPI, the magnetic signal from nanoparticles excited by a high-frequency harmonic field allows the users to determine their spatial distribution inside vessels or tissues by means of a tomographic procedure [14]. Medical applications include vascular imaging and visualization of internal organs, MPI being a promising alternative to techniques such as positron emission tomography and single-photon computed tomography which make use of radioactive tracers [15]. Although in some cases it could be advantageous to associate heating to tracing, in general MPI is intended to work as a diagnostic method with very limited or no impact on tissues or vessels. In this case, release of heat to the environment may be an undesired by-product of nanoparticle magnetic excitation. The short duration of a particle's excitation is often considered to guarantee that heating effects are negligible, although there is some controversy about this point, as well as indications that the problem may be underestimated [16]. Diagnostic MPI requires minimizing the heat released by excited nanoparticles.

Other biomedical applications, based on the displacement of particles by effect a magnetic field rather than on heating effects include blood detoxification by magnetic separation [17, 18] and magnetically-assisted haemodialisis [19]. In all cases involving the interaction of particles with living bodies, bio/haemocompatibility and biodegradability of magnetic particles play a most important role, as pointed out for various types of bare, coated, protein-conjugated magnetite nanoparticles [20, 21, 22, 23, 24, 25]

A radically different area of application of the heating properties of magnetically excited nanoparticles is the treatment of fluids in oil extraction industry (e.g., water-based/oil-based drilling fluids) and the active coating of the inner surfaces of tubing to eliminate hindrances to steady flow of oil (dewaxing). The heat delivered by the magnetic nanoparticles [2, 26] is exploited for flow assurance and improved production and transport of heavy oil.

In all these cases, an in-depth knowledge of the physical effects underlying the production of energy by magnetic nanoparticles is mandatory. Despite the ample literature on power generation by magnetically driven particles, this aim is still far from being accomplished. So far, expressions for the generated power based on the linear response theory [27] have been widely used; however, often the experimental or theoretical conditions do not allow one to freely make use of such an approximation [28]. At the present stage of scientific development, paralleled by a process of standardization of the techniques [28, 29, 30, 31], it is necessary to go beyond simplified theories by exploiting a more precise description of the physical mechanisms which govern the generation of energy by magnetic nanoparticles in order to obtain reliable predictions impacting present-day applications.

An important step forward towards a complete understanding of the processes leading to the production of heat by magnetization rotation or reversal in nanoparticles is based upon the recognition of the inherent complexity and non-linearity of the underlying physical effects which require to be studied from a physicist's standpoint [32].

In this work, a strategy aimed to modulate the ability of magnetic nanoparticles to release heat to an environment is proposed and discussed. We show that in the presence of dipole-dipole interaction nanoparticle clusters either enhance or reduce the released power with respect to a homogeneous distribution of particles, the fundamental parameters which determine the sign of the effect being the size of the nanoparticles and/or the dimensions of the clusters.

A simple model of compact (i.e., three-dimensional, non-dendritic) particle clusters is proposed. The average distance of individual nanoparticles inside a cluster is smaller than in the case of a homogeneous dispersion, so that dipole-dipole interaction among individual particles cannot be neglected. This paper is focussed on clusters with size of the order of some hundreds of nanometers containing from many hundreds to a few thousands particles. Examples of this type are not uncommon in the recent literature [33, 34, 35, 36, 37, 38, 39, 40, 41]. In this case, no direct simulation of the system by means of computational algorithms (e.g., by solving the LLG equations [42] or by using Monte-Carlo methods [43]) is possible, whereas this in the natural playground for an approximate approach based on rate equations [44, 45].

The effect of dipole-dipole interaction within a cluster is studied in the rate-equation framework by using a recent theory where the interaction is described as an additional contribution to the energy barrier between the two easy directions for the particle's magnetic moment [45, 46]. Rate equations determine the time evolution of the magnetization when the particles are excited by a high-frequency field, and allow one to draw the magnetic hysteresis loops. The loop area is proportional to the magnetic power released to the environment as heat.

The model predicts the changes of the hysteresis loops of clustered particles of magnetite (Fe_3O_4) which take place when the cluster size is ideally changed (magnetite nanoparticles are nowadays one of the most commonly used therapeutic agents in

nanobiomedicine owing to their biocompatibility). Monodisperse particles (i.e., all having the same size) with randomly distributed easy directions are studied first. It is shown that densely populated clusters are able to release an amount of thermal power markedly different from the one generated by homogeneous distributions. The same behaviour is observed not only for monodisperse nanoparticles but also in polydisperse systems, provided that the size distribution function is not too wide.

Therefore, the amount of released heat can be modulated, depending on one's needs and the specific application, by using fluid carriers or materials containing properly clustered instead than individual magnetic nanoparticles.

2. Model

2.1. Rate equations and dipolar interaction model

Rate equations have been shown to be particularly effective in the study of the behaviour of magnetic nanoparticles submitted to a magnetic field in the low to intermediate radio-frequency region ($f < 1$ MHz) [45, 47, 48]. In the rate-equation framework, the particles are viewed as classical two-well systems characterized by uniaxial magnetic anisotropy with randomly distributed easy axes. A summary of the distinctive features of this approach is found in the Supplementary Material (Section 1). The particles are assumed not to be physically displaced or rotated by effect of the driving field, as typically observed at high frequency and inside living bodies [49].

The dipolar interaction among nanoparticles is taken into account by adding a term to the standard expression of the energy barrier between the two wells, therefore approximating a multi-body problem in terms of a single-particle, mean-field theory, as discussed elsewhere [47, 50]. For particles made of magnetite (Fe_3O_4) with volume $V = \pi/6\, D^3$, D being the particle's diameter and magnetic moment $\mu = M_s V$ (M_s=350 kA/m [=350 emu/cm^3] being the saturation magnetization at room temperature) dispersed in a diamagnetic host, the maximum value of the additional contribution E_D^{max} to the local energy barrier of each particle is‡:

$$E_D^{max} = \frac{\mu_0}{4\pi}\,\alpha\frac{\mu^2}{d_0^3} = \frac{\mu_0}{4\pi}\,\alpha M_s^2 V \frac{V}{d_0^3} = \frac{\mu_0}{4\pi}\,\alpha M_s^2 V\, f_V \qquad (1)$$

where d_0 is the average interparticle distance, related to the volume fraction of particles dispersed in the host medium by the relation $f_V = V/d_0^3$ [45], and α is a numerical constant of the order of 10 deriving from the sum over the contributions of magnetic dipoles surrounding each particle [51]. The maximum value of the dipolar energy is attained when the dipoles are pointing towards all directions in space during a cyclic magnetization process (i.e., when the net magnetization of the material is equal to zero, corresponding to the coercive field on the hysteresis loop). When the dipoles are aligned by the applied field H, the dipolar energy takes a smaller value [52]; this

‡ in SI-units; equations in cgs-units are reported in the Supplementary Material, Section 8.

has been modelled by introducing an *ad-hoc* term in the expression of E_D [45], which finally becomes:

$$E_D(H) = \frac{\mu_0}{4\pi}\ \alpha M_s^2 V\,(1 - \frac{|m_0|(H)}{2}) f_V \tag{2}$$

where the alignment parameter $|m_0| = |M_0|/M_s$ is the absolute value of the reduced magnetization of a non-interacting system of monodisperse particles with random easy axes. This dimensionless quantity takes values between 0 and 1, being zero at the coercive field and unity at magnetic saturation ($H \to \infty$); when $H = 0$ it corresponds to the reduced remanence of the non-interacting loop. The above expression holds for ideally homogeneous or nearly-homogeneous nanoparticle systems.

The energy barrier $E_{B\,i}(H,\phi)$ of a two-well system whose easy anisotropy axis makes an angle ϕ with the magnetic field becomes therefore:

$$E_{B\,i}(H,\phi) = E^0_{B\,i}(H,\phi) + \frac{\mu_0}{4\pi}\ \alpha M_s^2 V\,(1 - \frac{|m_0|(H)}{2}) f_V. \tag{3}$$

$E^0_{B\,i}(H,\phi)$ is the height of the barrier for a non-interacting particle (as seen from potential well i, with i =1,2) and contains the product of the material's magnetic anisotropy K_u (2×10^4 J/m^3[$= 2 \times 10^5$ erg/cm^3] at room temperature for magnetite) times the volume V [46], so that the total energy barrier is directly proportional to the particle volume. The quantity $E^0_{B\,i}$ depends on angle ϕ when $H \neq 0$, by effect of the coupling energy term between particle's magnetic moment and the external field. The modified energy barrier regulates the time of jump of individual particles from one well to the other. The hysteretic magnetization is then obtained for each ϕ angle, and the $\phi-$dependent results are finally averaged over all angles between the anisotropy axis and the magnetic field [44].

In homogeneous systems, the effect of dipolar interaction is complex: the additional energy term, very sensitive to particle size and interparticle distance, turns out to either increase or decrease the area of the hysteresis loops generated in real applications [45, 53], therefore acting to enhance or reduce the thermal efficiency of an assembly of interacting nanoparticles.

The actual interval where magnetite particles excited at high frequency are able to generate a substantial amount of heat in typical operating conditions of *in vivo* applications is not particularly extended, being approximately in the 13-18 nm interval [47]. In fact, the constraints imposed by physiology require applying small fields when high frequencies are used in order to keep the product Hf sufficiently low [10], so that as a rule the particles are called to describe a *minor* hysteresis loop, i.e., one where the maximum magnetization (i.e., the magnetization measured at $|H_V|$) is very far from technical saturation.

It should be noted that in *major* hysteresis loops (where the maximum magnetization is at or very close to technical saturation), the loop's area is basically dominated by the coercive field $H_c^{(maj)}$, which at high operating frequency monotonically increases

with increasing particle size (see Supplementary Material, Section 2). On the contrary, the area of minor high-frequency loops is substantially different from zero only when the vertex field is of the same order of magnitude as the coercive field of the major loop, i.e., $H_c^{(maj)} \simeq H_V$ [45]. There is a limited interval of particle sizes where this condition is fulfilled; for values of D outside this interval, the loops are very narrow and the associated area very small. The point is made clear in the Supplementary Material.

In a polydisperse system characterized by a distribution function of particle sizes $p(D)$ and a random distribution in space of particles having different sizes, with average interparticle distance $\overline{d_0}$, Equation (3) is substituted by [45]:

$$E_{B\,i}(H,\phi) = E^0_{B\,i}(H,\phi) + \frac{\mu_0}{4\pi}\,\alpha M_s^2 \frac{\overline{V^2}}{\overline{V}}\,(1 - \frac{\overline{|m_0|}(H)}{2} f_V, \tag{4}$$

where $\overline{V} = \int V p(D) dD$, $\overline{V^2} = \int V^2 p(D) dD$, and use has been done of the relation $f_V = \overline{V}/\overline{d_0}^3$. The dipolar energy is still given by Equation (1) where $\mu^2 \to \overline{\mu^2} = M_s^2 \overline{V^2}$. Here $\overline{|m_0|}$ is the absolute value of the average reduced magnetization of size-distributed, non-interacting particles. The resulting hysteresis loops are first averaged over ϕ and finally summed up using $p(D)$ as weight function.

As a final remark, the rate equation approach cannot be indiscriminately exploited to describe the behaviour of magnetic nanoparticles of arbitrary size [8]. In principle, rate equations approximate the Fokker-Planck equation for the double-well problem when the ratio $E_{B\,i}/k_BT$ is larger than unity [54]; however, they were shown to be still useful when $E_{B\,i}/k_BT \simeq 0.92$ or just below [54]. As a consequence, at each temperature there is a lower limit to the diameter of nanoparticles which can be analysed by the rate equation method. Taking $E_{B\,i} = E^0_{B\,i} = K_u V$, the limit is expressed by the condition $D \gtrsim (5.52\, k_BT/\pi K_u)^{1/3}$. In the present case, around room temperature the lower limit turns out to be $D \simeq 7.5$ nm, so that the diameter D of the studied particles is equal to or larger than 8 nm.

2.2. Modeling nanoparticle clusters

We study the effect of inhomogeneities in the space distribution of magnetic particles on the hysteresis loops and the resulting heating efficiency, without however investigating the microscopic causes leading to the development of inhomogeneities (which can be of electrical, magnetic, chemical nature). Inside a cluster the magnetic particles are assumed to be still isolated, i.e. not in physical contact (in order to exclude magnetic contact interaction such as the exchange interaction); however, the interparticle distance d is much shorter than the one existing in a homogeneous system with the same volume fraction, so that the dipole-dipole energy, proportional to d^{-3}, is much stronger. On the other hand, clusters are assumed to be well separated from each other, so that dipolar interactions between any two of them can be neglected as a first approximation.

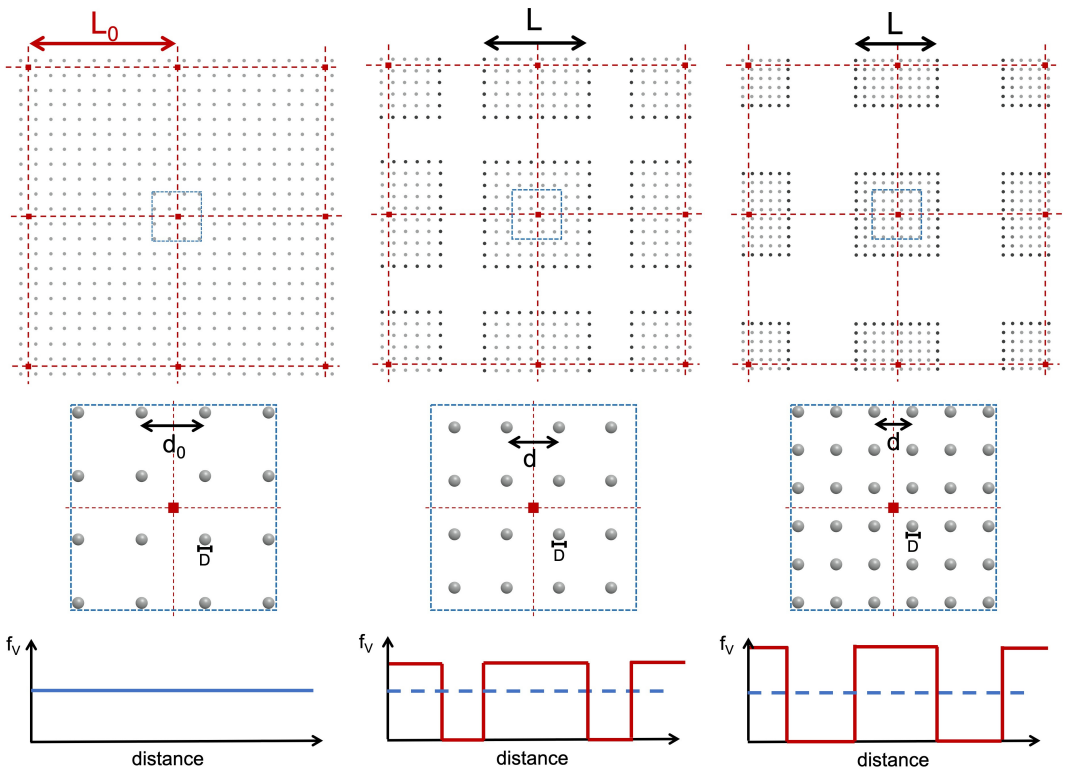

Figure 1. Two-dimensional sketch of idealized particle clustering. Each dot of the array represents a magnetite nanoparticle of diameter D. Left panel: uniform distribution of particles with mean distance d_0. Centre and right panels: two different stages of the formation of clusters of side L. The second row shows for all cases an enlargement of the region outlined in blue in the first row. The behaviour of the density of particles is schematically shown in the third row.

We consider monodisperse particles first. The development of clusters from an initially homogeneous distribution of particles is figured out as follows (see Figure 1, where for simplicity the two-dimensional case is depicted):

- homogeneously dispersed particles of diameter D are first placed on a simple cubic lattice whose nearest-neighbour distance is $d_0 = (V/f_V)^{1/3}$ (upper left panel of Figure 1; the intermediate left panel shows an enlarged view of the immediate surroundings of any particle);
- the length $L_0 = Nd_0$ is introduced, with $N >> 1$ (two cases [$N = 10$ and $N = 20$] will be considered in the following); the system of nanoparticles can therefore be viewed as an assembly of juxtaposed, identical cubes of side L_0; the length L_0 is linked to the number of particles in a cluster, $N^{(cl)} = (N+1)^3 \simeq L_0^3 f_V/V$;
- the size of each cube is then uniformly reduced along three dimensions by keeping the initial distance between centres (L_0); the side length becomes $L < L_0$ (centre panels of Figure 1); within a cluster the interparticle distance is now $d < d_0$, with $d = L/N$;

- during the process the center-to center distance between adjacent clusters remains fixed at L_0;
- the process is carried on until a minimum interparticle distance is attained (right panels of Figure 1);
- the cubic clusters are assumed to be separated by a face-to-face distance $L_0 - L$ such that they can be considered as non-interacting. This means that the actual arrangement of the clusters within the material is unimportant, i.e., the model's results do not depend on the more or less regular separation between clusters;
- the *average* density of particles in the host material (parameterized by the volume fraction f_V) is always the same and equal to V/d_0^3; however, within a cluster the local density becomes $f_V^{(cl)} = V/d^3$ while outside it drops to zero, each cluster being surrounded by a region of material where there are no particles; this is schematically shown (in one dimension) in the bottom line of Figure 1.

We explicitly acknowledge that this highly idealized mechanism of particle clustering is not a description of the actual processes of cluster formation in real materials, which are usually driven by physical or chemical mechanisms including interaction with hydrophobic blocks of copolymers [33, 41] or microgels [34, 38], alternating magnetic field assisted co-precipitation [35], solvothermal reactions [36] and surfactant-assisted synthesis [37]. However, our model has the advantage of providing a simple way to understand how and how much does dipolar interaction affect the magnetic behaviour of clusters of different size. Using a different spatial arrangement of nanoparticles does not to entail substantial differences with respect to this model (see Supplementary Material, Section 3).

These cubic particle clusters contain $(N+1)^3$ particles whose distance is lower than d_0 and are separated by extended regions of non-magnetic material. The model can be applied to describe the magnetic properties of arrays of dense, isotropic clusters of particles, often observed in the literature [33, 34, 35, 36, 37, 38, 39, 40, 41], whilst cannot be directly applied to describe irregular or fractal clusters [55] or linear chains [56].

Both an upper and a lower limit to cluster size can be defined. The lower limit of L derives from the requirement that the dipolar energy should not exceed a maximum threshold in order to apply the mean-field approach of Equations 1 and 2. In particular, the maximum dipolar energy defined in Equation 1 must not be much larger than the barrier arising from the particle's magnetic anisotropy [57], which is equal to $K_u V$ when $H = 0$. Requiring that $E_D^{max} \lesssim 2\,K_u V$ implies that the condition $\frac{\mu_0}{4\pi}\alpha M_s^2 f_V \lesssim 2\,K_u$ must be satisfied; this results in the following condition on the interparticle distance d:

$$d \gtrsim d_{min} = \left(\frac{\mu_0\,\alpha M_s^2}{48 K_u}\right)^{1/3} D \tag{5}$$

With the parameter values used in this work, the condition becomes $d \gtrsim 1.17\,D$. As a consequence, we require that d not to be less than $d_{min} = 1.2\,D$, so that $L \geq 1.2\,N D$.

The upper limit of L derives instead from the requirement that the clusters must

be separated from each other so that the dipolar interaction between any two of them is negligible. The existence of an effective cutoff length for dipole-dipole interactions among magnetic nanoparticles has been inferred by theoretical considerations [45] and substantiated by measurements [58, 59]. In particular, the cutoff length λ is of the order of $4\,D$ at f =100 kHz, i.e., at the magnetizing frequency used in this work [45]. In other words, magnetic particles separated by a distance equivalent to four diameters or more can be assumed as non-interacting. An explicit proof can be found in the Supplementary Material, Section 4. It is therefore required that two neighbouring cubes of size L are placed at a face-to-face distance such that $L_0 - L > 4\,D$, which can be transformed into the condition $d < d_{max} = d_0 - 4D/N$.

In the following, the model will therefore be applied by requiring that the interparticle distance within a cluster d varies in the range $1.2\,D \leq d \leq (d_0 - 4D/N)$.

2.3. Dipole-dipole interaction in a cluster

Within a cluster, the dipole-dipole interaction is generally enhanced by the reduction of the interparticle distance. However, a distinction has to be made between core and surface effects. In fact, particles present, e.g., on the cube's face experience a reduced dipolar interaction because of the lack of translational symmetry. An example is shown in Figure 2, where the left panel refers to a particle in the cluster's core and the right panel to a particle on any of the cube's faces. In both cases, the reference particle (in red) is surrounded by magnetic dipoles placed on the $1^{st}, 2^{nd}, 3^{rd}$ ... neighbour lattice sites and concurring to determine the value of the dipole-dipole energy on it. For simplicity of representation, only the first three neighbours are highlighted in different colours. The actual counting of active neighbours takes into account the requirement that their distance from the centre has to be smaller than $\lambda = 4\,D$, as previously discussed; it should be noted that the actual number of dipoles giving a nonzero contribution to the dipolar energy increases with reducing the cluster size, i.e., the inner interparticle distance d.

The dipole-dipole energy of a core particle (panel *a*) and of a particle placed either on a face (as in panel *b*), or an edge or a vertex of the cube is assumed to be determined by the number of active neighbours, which is different in each case (core, face, edge, vertex). The assumption can be justified by recalling that the parameter α appearing in Equation 1 actually contains a summation over all active neighbours [51] of the reference particle.

Therefore, if the number of active neighbours for a particle placed on a cube's face is n_f and the one for a core particle is n_c, with $n_f < n_c$, the dipolar energy on the former particle is assumed to be simply reduced by a factor n_f/n_c with respect to the one of a core particle. It should be noted that a decrease in the number of active neighbours is observed not only for the particles on the outer layer of the cube, but also for the ones present on the second layer from outside.

As a consequence, the energy barriers are different for two-level systems in the core

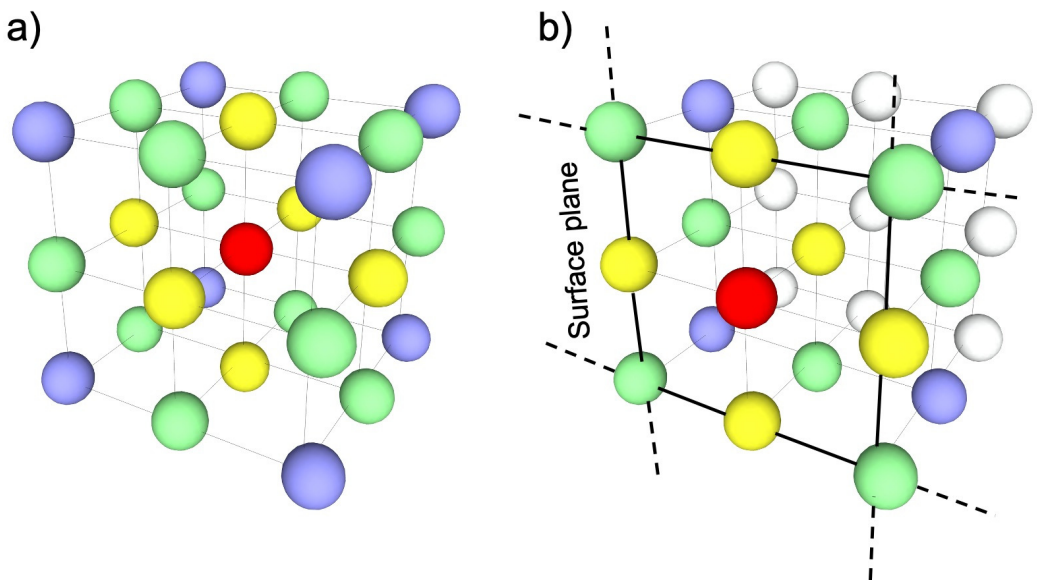

Figure 2. First, second, third neighbours (spheres in yellow, green, violet) of a reference particle (in red) placed either in the cluster's core (panel *a*) or on one of the cube's faces (panel *b*). The overall number of active neighbours on the face is always smaller than the one in the core.

and at the cluster's surface (this term grouping all layers interested by any reduction of the number of active neighbours), so that the kinetics of redistribution of the population between the two energy wells is different from core to surface. The overall cluster's contribution is therefore obtained by doing the weighted sum of the results obtained for all types of surface and core particles, the weights being given by the ratios between the number of particles of each type divided by the total number of particles in the cluster: as an example, when the surface is comprised of the first two outer layers of a cube of size $L = Nd$ made of $(N+1)^3$ particles there are $(N-3)^3$ particles in the core and 8 particles on the outer vertexes, so that the weight of the contribution from core particles is $(N-3)^3/(N+1)^3$, whilst the one from the outer vertex particles is $8/(N+1)^3$, and so on for all particles belonging in the two outer layers.

3. Results and Discussion

Room-temperature magnetic hysteresis loops of particle clusters are computed by numerically solving the rate equations [44] under a harmonic magnetic-field waveform of frequency $f = 100$ kHz with vertex field $H_V = 7.958$ kA/m (=100 Oe). It should be stressed that the considered loops are *minor* loops. In actual applications of magnetic particles for hyperthermia in living bodies it is strictly required that the vertex field be kept as low as possible, so that minor hysteresis loops are typically generated [60].

The volume fraction of magnetite nanoparticles dispersed in the host medium is

$f_V = 0.01$, a value corresponding to a rather small amount of magnetically active material when particles are homogeneously dispersed; notice that this value remains the same on the average even in the presence of clustering, although within a cluster the local volume fraction is much higher. All parameter values closely correspond to the ones typically found in *in vitro* and *in-vivo* applications of magnetic hyperthermia [10].

3.1. Clusters of monodisperse particles

Examples of the effect of particle clustering on the shape of the high-frequency hysteresis loops with vertex field $H_V = 7.958$ kA/m (100 Oe) are shown in Figure 3 for monodisperse magnetite particles of three different diameters (note that the dipolar energy term E_D increases with increasing D as $\mu^2 \sim D^6$). The cluster size is equal to $N = 10$ interparticle distances, so that each cluster contains $(N+1)^3 \simeq 1.33 \times 10^3$ particles.

Figure 3 shows that particle clustering strongly modifies the hysteresis loop's area A_L and consequently the heating efficiency of the nanoparticle assembly. In magnetic hyperthermia, a typical figure of merit is the Specific Loss Power (or SLP) defined as the power released by the nanoparticles divided by their total mass [10]. The Specific Loss Power (W_{SLP}) is directly proportional to the loop's area A_L measured at a given frequency f according to the relation $W_{SLP} = f_V A_L f/\rho_{Fe_3O_4}$ [10] where $\rho_{Fe_3O_4} \simeq 5240$ Kg/m^3 is the mass density of magnetite.

The behaviour of the loops of Figure 3 is explained taking into account the complex effects of dipolar interaction on the width of hysteresis loops, which were clarified elsewhere [45]. In brief, the widest hysteresis loop is expected - for a given frequency f and vertex field H_V - when the typical time of jump across the energy barrier (τ) is roughly equal to the driving field period $1/f$. At constant temperature, the value of τ is determined by the particle diameter, D, and by the strength of dipolar interaction (which monotonically increases with decreasing cluster size L), so that a very wide hysteresis loop emerges for one (and only one) pair of values of D and L, which makes the height of the energy barrier such that the condition $\tau \simeq 1/f$ is fulfilled. The three cases shown in Figure 3 are discussed in more detail in the following paragraphs.

When $D = 10$ nm, the interparticle distance for the homogeneous particle dispersion is $d_0 = (V/f_V)^{1/3} \simeq 37.4$ nm. At the operating frequency, the hysteresis loops are observed to be extremely narrow for both the homogeneous dispersion and all cluster sizes; in fact, for large interparticle distances the magnetization is nearly anhysteretic (left panel, red and green line); the dipolar interaction, which increases with decreasing L as $E_D \sim d^{-3} \sim L^{-3}$, is always very small and begins to play a barely discernible role for the smallest studied cluster size only ($L \simeq N d_{min} \simeq 1.2ND$), resulting in a narrow closed loop (black line). In this case, the condition $\tau \simeq 1/f$ is never fulfilled in the range of validity of the model.

When $D = 13$ nm, $d_0 = (V/f_V)^{1/3} \simeq 48.6$ nm. In this case, the SLP is initially strongly

enhanced by particle clustering (compare green and red lines in centre panel): dipolar interaction, strengthened by the reduction of the interparticle distance, increases both the coercive field and the magnetic remanence of the loops, making them much wider than the ones found in the homogeneous dispersion or in very large clusters. However, further reducing the cluster size (and the associated interparticle distance) a sharp reduction of W_{SLP} (black line) is observed. Therefore, a maximum of the SLP exists for an intermediate cluster size, where the condition $\tau \simeq 1/f$ is fulfilled.

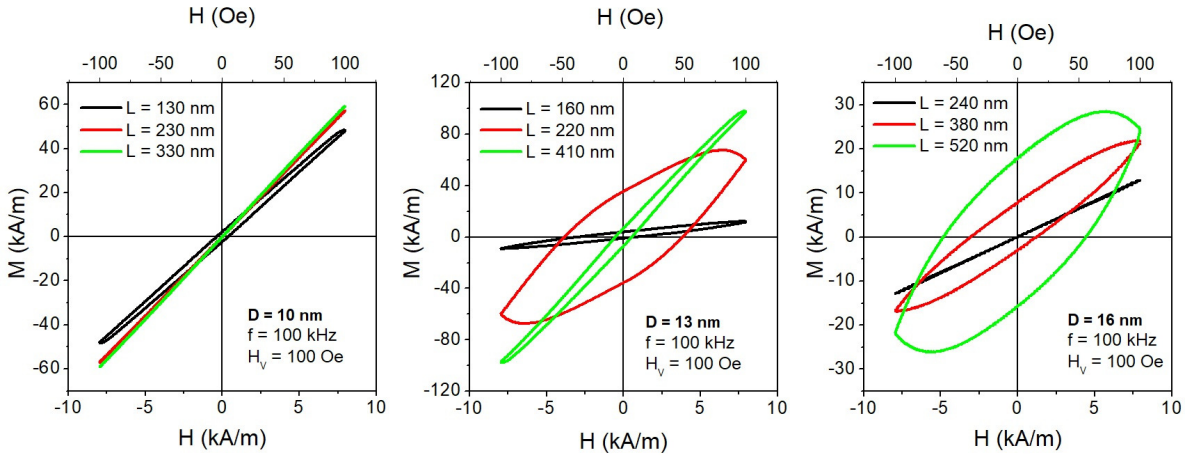

Figure 3. Minor hysteresis loops of magnetite particle clusters computed at $f = 100$ kHz for three values of the cluster size L. Left: particle diameter $D = 10$ nm; center: $D = 13$ nm; right: $D = 16$ nm. Vertex field $H_V = 7.958$ kA/m (100 Oe) in all cases.

When $D = 16$ nm, the homogeneous interparticle distance is $d_0 \simeq 59.9$ nm. In the homogeneous sample the SLP is large and monotonically decreases with decreasing cluster size. In this case, the condition $\tau \simeq 1/f$ is fulfilled for the homogeneous system only.

Therefore, particle size plays an importantl role on the effects on W_{SLP} arising from clustering. An example of the complete behaviour of the SLP as a function of cluster size over the entire interval of validity of the model is reported in the left panel of Figure 4 for $D = 13$ nm and for clusters characterized by $N = 10$ and 20 (black/red symbols, respectively). The SLP values of homogeneously dispersed and non-interacting particles are also shown (dark green symbol at right bottom, and dashed horizontal line, respectively). For the considered value of f_V the effect of dipolar interactions in the homogeneous dispersion is small and produces a modest increase in the heating efficiency with respect to the non-interacting case; however, when particle clusters begin to be formed, the heating efficiency is enhanced, reaching a value almost seven times higher than in the homogeneous system. Finally, when the cluster size becomes so small that d approaches d_{min}, W_{SLP} begins to decrease by effect of the increase in dipolar energy which takes place at small interparticle distance. Figure 4 indicates that the parameter most affecting the $W_{SLP}(L)$ curve for particles of diameter D is the interparticle dis-

tance in a cluster, d, rather than cluster size. However, a lesser role is also played by the number of particles comprised in a cluster, because of the edge effects related to the smaller dipolar interaction existing at the cluster's surfaces. Edge effects play a greater role for small N and are responsible for the difference between the two curves shown in the left panel of Figure 4; the behaviour of additional W_{SLP} curves for $10 \leq N \leq 100$ is reported in the Supplementary Material, Section 5. The distinctive features of the W_{SLP} curves (e.g., maximum value of W_{SLP}, position of the maximum, width of the peak) are markedly influenced by the particle diameter, as also shown in the Supplementary Material. This is related to the fact that a change of D modifies the dipolar energy contribution as D^2 for any value of the interparticle distance d.

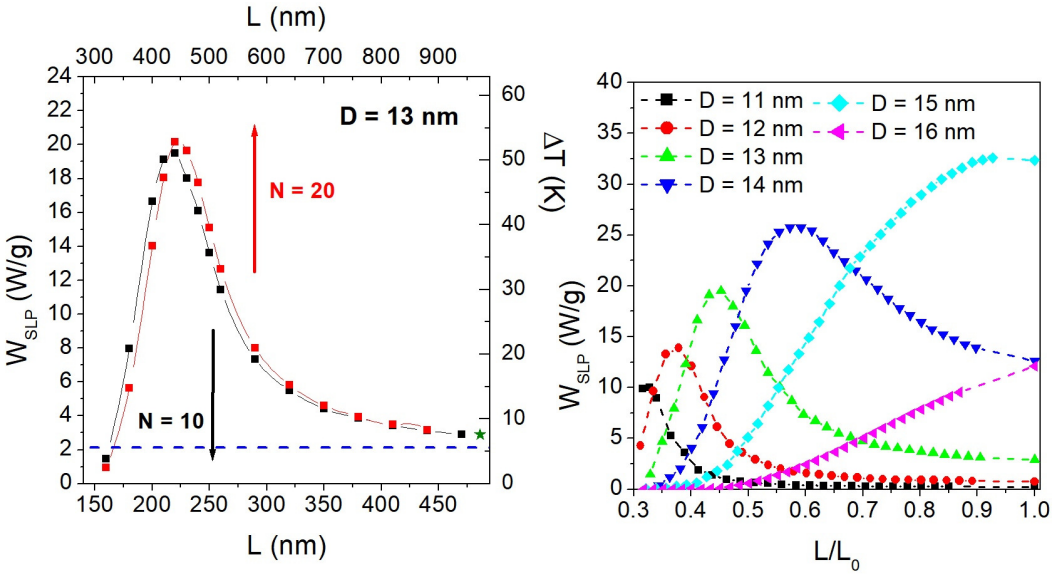

Figure 4. Left panel: behaviour of the specific loss power W_{SLP} as a function of the cluster size for two different clusters of 13-nm magnetite nanoparticles with ($N = 10$ and $N = 20$). Shown at bottom right is the value for the homogeneous distribution The temperature increments shown on the right vertical axis have been estimated using a simple model of heating (see Section 3.4) . Right panel: effect of particle clustering on W_{SLP} as a function of the reduced cluster size L/L_0 for different particle diameters (the points at $L/L_0 = 1$ are the W_{SLP} values of the homogeneous distributions; the dotted lines are guides for the eye).

The right panel of Figure 4 shows the role of particle size on the variation of the SLP by effect of particle clustering (with $N = 10$). In order to compare datasets arising from different values of D the reduced cluster size L/L_0 is used (remember that $L_0 = Nd_0 = N(V/f_V)^{1/3}$). The points at L/L_0=1 correspond to the values obtained for homogeneously dispersed particles. It should be remarked that for $D \lesssim 10$ nm the magnetization curves are basically anhysteretic not only for the homogeneous dispersion but also for all explored cluster sizes, so that the W_{SLP} is basically zero throughout.

For the considered L/L_0 values, corresponding to the region where the model can be applied, W_{SLP} steadily decreases with decreasing cluster size when $D \geq 16$ nm. In the interval $12 \leq D \leq 15$ nm the SLP first increases with decreasing L/L_0 and is reduced when the reduced cluster size becomes small. When $D < 12$ nm, W_{SLP} steadily increases with decreasing cluster size. Such a behaviour is clearly related to dipole-dipole interaction, as discussed in Section 2.1. Generally speaking, particle clustering results in an enhanced thermal efficiency of small particles packed in dense clusters, whilst the opposite is true for large particles. The change takes place gradually with increasing D.

3.2. Cluster size maximizing the SLP

The effects described in the previous Section can be quantitatively described taking into account the ratio between the Néel relaxation time, i.e., the mean time between two flips of the magnetization across the barrier, to the driving field's period. The behaviour of W_{SLP} with the volume fraction of homogeneously dispersed particles was discussed elsewhere [45]. There, taking into account the relation between f_V and the interparticle distance d, it was shown that the curve $W_{SLP}(f_V)$ displays a single maximum corresponding to an interparticle distance such that the typical relaxation time τ is of the order of the period of the driving field, $1/f$.
In the present case, although the overall volume fraction is always the same, the interparticle distance d depends on the size of the clusters. The value of d corresponding to the maximum of W_{SLP} is found by imposing the standard condition $\tau = \tau_0 \, exp\left[\frac{E_B(d)}{k_B T}\right] \simeq 1/f$ [47] where $\tau_0 \sim 10^{-9}$ s is the reciprocal of the attempt frequency and E_B is the height of the energy barrier at $H = 0$, which is a function of f_V and therefore of d through the dipolar energy term (see Equation 3). The cluster size $L^{(Max)}$ where W_{SLP} takes the maximum value turns out to be:

$$L^{(Max)} = N d^{(Max)} = \frac{N}{2}\left\{\frac{\alpha M_s^2 \pi}{18\left[k_B T ln(1/\tau_0 f) - (\pi/6) K_u D^3\right]}\right\}^{1/3} D^2. \qquad (6)$$

This equation is valid only for values of D such that the denominator of the expression in braces is positive. When the denominator goes to zero, the optimal interparticle distance $d^{(Max)}$ diverges, which in the model's language means that W_{SLP} would be largest for an infinitely dilute, non-interacting system (the dipolar interaction disappears in the limit of an infinite interparticle distance).
The behaviour of $L^{(Max)}$ as a function of particle diameter D is shown in the left panel of Figure 5. The two shaded regions indicate the zones where Equation 6 cannot be applied. In fact, the lower region is bounded by the $L = N d_{min} \simeq 1.2ND$ line (see Equation 5) whereas the upper region is bounded by the $L = L_0 \equiv N d_0$ line, corresponding to the homogeneous dispersion of particles.

In Figure 5, the red curve merges with the $L = 1.2ND$ line for $D \lesssim 11$ nm: in this case, $d^{(Max)} = d_{min}$, because the real absolute maximum of the $W_{SLP}(L)$ curve would

occur at a distance $d < 1.2\,D$, where the model is no longer applicable. In this interval of particle sizes, the $W_{SLP}(L)$ curve monotonically increases with decreasing L.

On the other hand, the red curve merges with the $L = L_0$ line for $D \gtrsim 15$ nm: for large particle sizes the SLP is largest for the homogeneous dispersion, and clustering reduces the heating ability of nanoparticles. Only in the interval $11 \lesssim D \lesssim 15$ nm there exists an intermediate distance $d^{(Max)}$ and an associated cluster size $L^{(Max)} = Nd^{(max)}$ where the $W_{SLP}(L)$ curve displays an absolute maximum.

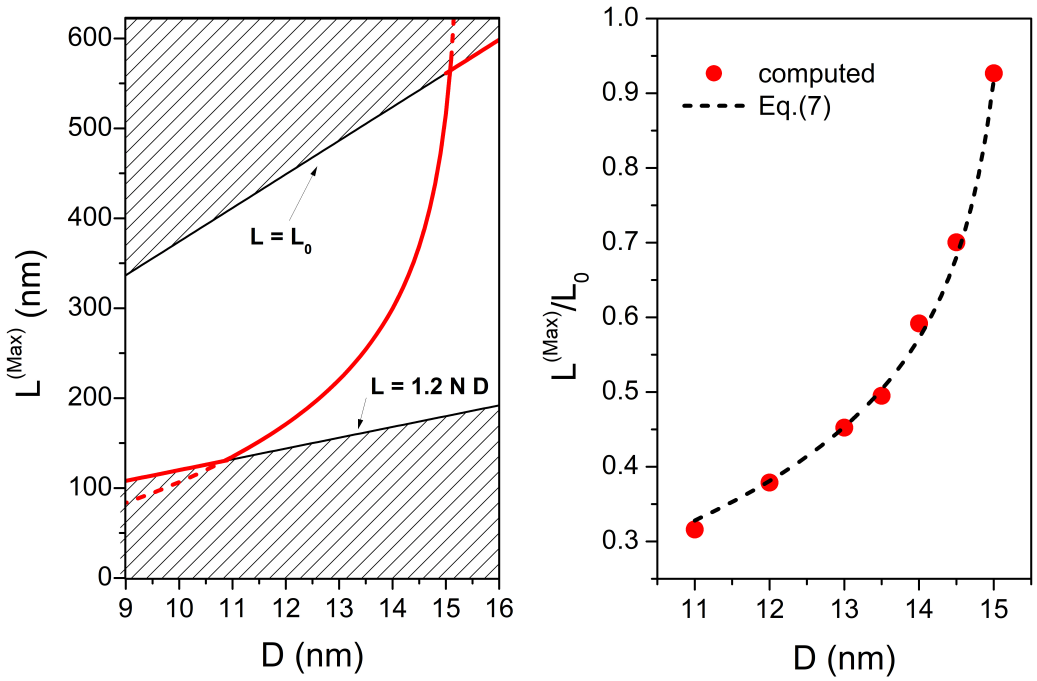

Figure 5. Left: Optimal cluster size $L^{(Max)}$ corresponding to the maximum SLP as a function of particle size D, according to Equation 6 (red line). Patterned areas: regions where the analytic expression cannot be applied (see text). Right: comparison between the values of the ratio $L^{(Max)}/L_0 \equiv d^{(Max)}/d_0$ predicted by Equation 7 and observed in the computed $W_{SLP}(L)$ curves.

The ability of Equation 6 to actually predict the position of the maximum SLP can be checked by dividing the expression for $L^{(Max)}$ by $L_0 = Nd_0 = N(\pi/6f_V)^{1/3}D$:

$$\frac{L^{(Max)}}{L_0} = \frac{d^{(Max)}}{d_0} = \frac{1}{2}\left\{\frac{\alpha M_s^2 f_V}{3\left[k_B T ln(1/\tau_0 f) - (\pi/6)K_u D^3\right]}\right\}^{1/3} D. \qquad (7)$$

The behaviour of $L^{(Max)}/L_0 = d^{(Max)}/d_0$ with diameter D is shown on the right panel of Figure 5 (black dashed line) and the actual maxima of the W_{SLP} curves simulated in the same interval of D values (including the ones shown in the right panel of Figure 5) are plotted as red circles. The agreement between the analytic expression and the results of numerical computation is very good, indicating that the application of the

model gives self-consistent results.

3.3. Particle size and maximum possible enhancement/reduction of the SLP

The effect of particle size on the maximum possible enhancement of the SLP by particle clustering is depicted in Figure 6 (black open symbols in the left panel). By "maximum possible enhancement" it is meant here that there exist one size of the clusters, $L^{(Max)}$, for which the SLP takes the highest possible value $W_{SLP}^{(Max)}$ for a given particle size.

As previously discussed, an absolute maximum of the $W_{SLP}(L)$ curve is found for particle sizes larger than $D = 11$ nm only; therefore, this region is shown in Figure 6. The red circles represent the W_{SLP} values obtained for homogeneously dispersed particles. When D is decreased from $D = 18$ nm to 11 nm, $W_{SLP}^{(Hom)}$ increases, reaches a maximum for D close to 15 nm, then decreases and becomes rapidly negligible. Such a behaviour has been explained in detail elsewhere [45] and was briefly discussed in Section 3.1. A sharp maximum of $W_{SLP}^{(Hom)}$ is found when the hysteresis loop is very wide; in turn, the loop is widest when the typical time of jump across the energy barrier (τ) becomes roughly equal to the driving field period $1/f$ (the condition is verified, for a homogeneous system, when $D \simeq 15$ nm).
On the contrary, the open symbols represent the $W_{SLP}^{(Max)}$ values predicted in clustered systems. It is observed that for $D \gtrsim 15$ nm the two datasets are perfectly coincident: this means that particle clustering does not give a better SLP than the one of the homogeneous dispersion (actually, clustering decreases the SLP in this region). Below 15 nm, however, the values of $W_{SLP}^{(Max)}$, although decreasing with decreasing D, remain significanty higher than the ones of $W_{SLP}^{(Hom)}$. This means that in this region the formation of clusters of suitable size permits to effectively enhance the heating ability of nanoparticles.

No exact analytic expression of $W_{SLP}^{(Max)}$ can be derived from the rate equations; however, its functional dependence on particle size D can be determined by exploiting the condition $\tau \simeq 1/f$, as discussed in the Supplementary Material, Section 6. In particular, in the interval of validity of Eq.6 the functional dependence of the maximum SLP on D turns out to be of the type:

$$W_{SLP}^{(Max)}(D) = \frac{a}{1 + exp(-\beta D^3)} - c \tag{8}$$

Meaning and values of the constants $a, \beta, c \simeq a/2$ are discussed in the Supplementary Material. The values of $W_{SLP}^{(Max)}$ obtained from the numerical solution of the rate equations are well fitted by Eq. 8 (dashed blue line in Figure 6) with the following parameter values: $a = 191.90$ W/g, $\beta = 2.55 \times 10^{17}$ cm^{-3}, $c = 102.38$ W/g. It should be noted that while the calculation done in the Supplementary Material does not permit to obtain the values of constants a and c which are adjustable parameters derived from the fit, the quantity β, instrumental in determining the functional dependence of $W_{SLP}^{(max)}$ on

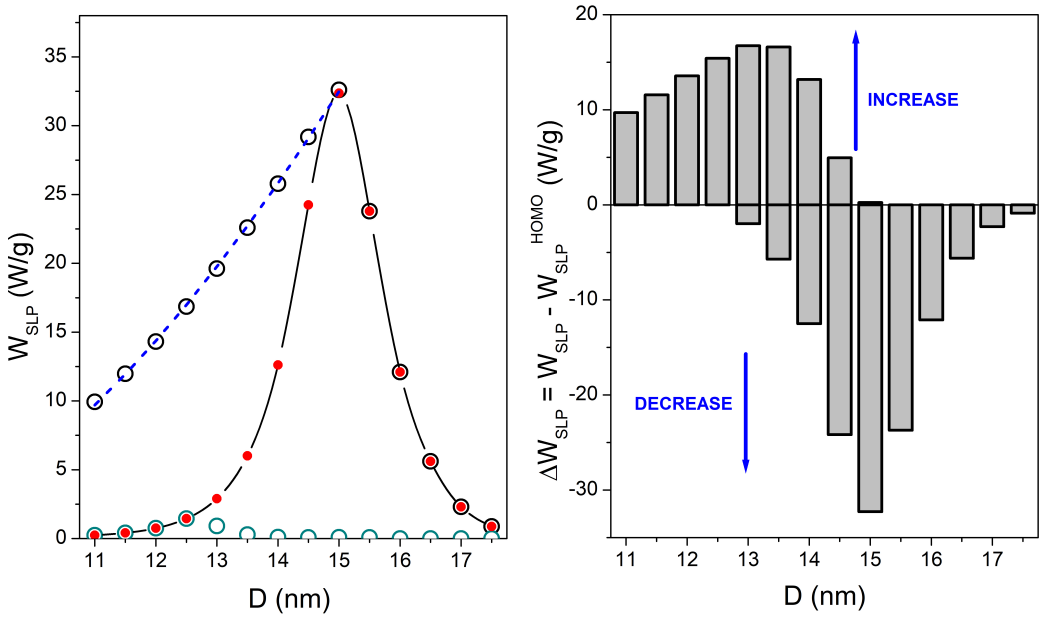

Figure 6. Left panel: red circles: SLP as a function of particle size in the interval 11 $\leq D \leq$ 16 nm for homogeneously distributed particles; black open circles: maximum possible SLP for clustered particles in the same range; dashed blue line: fit to Eq. 8; green open circles: minimum possible SLP for clustered particles. Right panel: tunability of the SLP as a function of particle diameter D; ΔW_{SLP} is the difference between the SLP of clustered and homogeneously distributed particles.

D, is accurately predicted by the calculation.

On the other hand, in view of diagnostic applications such as MPI, it may be interesting to study under which conditions the more effective *reduction* of the SLP on clustering is to be expected. The results are also shown in the left panel of Figure 6 (green open symbols). For low particle sizes ($D \leq 12.5$ nm) the minimum possible value of the SLP ($W_{SLP}^{(Min)}$) corresponds to the homogeneous dispersion of particles; for higher D values particle clustering brings about a substantial reduction of the SLP with respect to the homogeneous case, so that $W_{SLP}^{(Min)}$ becomes very close to zero.

A suitable graphical representation of the SLP modulation by effect of particle clustering is shown in the right panel of Figure 6. The quantity $\Delta W_{SLP} = W_{SLP} - W_{SLP}^{(Hom)}$ measures the positive and/or negative variation of the SLP produced by clustered particles with respect to the homogeneous case, which is taken as a baseline. The parameter ΔW_{SLP} helps clarify the different behaviour of particles in dependence of their size: small particles ($D \leq 12.5$ nm) can only increase their SLP on clustering, whereas cluster formation can only reduce the SLP of large particles ($D \gtrsim 15$ nm). For intermediate values of D (in the present case, around 14 nm) clustering of particles may either en-

hance or reduce the SLP with respect to the homogeneous case, depending on the size of clusters. From this viewpoint, this is the particle size which ensures the best tunability of the SLP.

The model's features can be discussed along with the ones of recent approaches to the properties of compact particle clusters, based either on numerical solutions of the LLG equation [42, 61, 62, 63] or Monte-Carlo simulations [43, 64, 65, 66].

In some simulations the effects of interactions inside the clusters are not considered in detail [67, 68]. In other papers, a strictly linear approach is adopted to describe magnetization processes leading to the production of energy by clustered particles [68, 69, 70]). In all cases the simulations are necessarily aimed to describe very small clusters, the number of individual particles per cluster never exceeding one hundred, and often being significantly lesser. In principle, the present method poses no limits to the size of clusters, takes into account the interactions inside clusters in an effective way, and is able to provide reliable results even in the operating conditions of therapeutic hyperthermia where the linear model is no longer applicable, resulting in an imprecise temperature estimate [47].

Some recent numerical results appear to be either not entirely explained (e.g., the maximum of the SLP for a specific interparticle distance in a cluster [61]) or contradictory (e.g., the contrasting conclusions that SLP is not affected by particle clustering [64, 63] and that in isotropic clusters it is lower than in individual particles [42, 43], whereas some measurements do show an increase of SLP on clustering [33, 41]). These issues can be coherently explained by the present approach, which is based on an accurate representation of particle magnetization and is remarkably flexible, in the sense that the relevant physical parameters can be modulated more freely than in strictly numerical methods.

3.4. Particle clustering and temperature increment

The temperature increment measured during the heating process of a diamagnetic host medium is modified by nanoparticle clustering as a consequence of the effects on the SLP we have just described. Specific features of magnetic hyperthermia achieved using either non-interacting or interacting particles have been discussed in detail elsewhere [45, 47]. Here, an approximate estimate of the temperature achieved by a sample containing a fraction $f_V = 0.01$ of magnetite nanoparticles, either evenly dispersed or forming clusters, is done using the simple approach outlined in the Supplementary Material, Section 7, where the time- and space-dependent temperature increment resulting by excitation of clustered particles is discussed. A typical result is reported on the right vertical axis of Figure 4, left panel. It can be concluded that particle clustering can significantly improve the target temperature with respect to the homogeneous case.

Looking for the most convenient use of clusters of particles, a simple rule of thumb is given here: if magnetite particles larger than 14-15 nm are being considered for

practical application requiring a high SLP, the best strategy is to have a homogeneous dispersion in, or around, the target tissue; conversely, if the particles are in the 11-14 size range, particle clustering offers a definitely advantageous way to increase the heating performance without the need of using a large amount of inoculated metal ions.

As a matter of fact, many different sizes of iron oxide nanoparticles have been considered for practical, i.e., *in-vivo* applications of magnetic hyperthermia [7]. On the basis of physiology considerations, particle diameters between 12 and 50 nm have been indicated as ideal for application in biomedicine, the lower limit being dictated by the requirement that the particles should be large enough so that they do not cross the pores of a blood vessel wall, which are typically smaller than 12 nm [71]. The upper limit is instead defined with reference to the ease of transport in the blood circulation [71]. Let us stress, however, that magnetite particles larger than 18-20 nm (depending on the parameter values) are basically ineffective as heaters of a living tissue when submitted to a radio-frequency magnetic field whose amplitude is sufficiently small to be tolerated by patients [10].

Magnetic fluid hyperthermia has been demonstrated and used in actual clinical trials using 12-13 nm magnetite nanoparticles with a bio-compatible coating (NanoTherm (R), [72]). However, in this case the solution is usually inoculated at a high concentration of 112 mg/mL of iron [72], corresponding to a magnetite particle volume fraction $f_V \simeq 0.03$, because a large local amount of magnetite is needed to achieve thermal tissue ablation. When small particles are to be used, particle clusters of suitable size can provide a superior heating efficiency, allowing one to significantly reduce the amount of particle concentration in the magnetic fluid and avoid the detrimental consequences of the inoculation of a high volume fraction of nanoparticles in a living body.

On the other hand, use of magnetite nanoparticles in MPI of both healthy and diseased tissues [5] may imply applying frequencies and amplitudes of the magnetic field such that local heating of the tissue - which is an undesired by-product of the technique in this case - cannot be disregarded [16]. In the light of the present analysis, such a by-product could be avoided by dispersing compact clusters of large ($D > 15$ nm) particles in the tissue, instead of using single particles. In this case the magnetic interactions within clusters located at the field-free point (or line) of the MPI scanner [5] will substantially reduce the hysteresis loops' area keeping the released heat low, while the signal generated by the switching cluster magnetization and exploited to produce the tomographic image is expected to remain easily detectable by a typical MPI setup.

3.5. Clusters of polydisperse particles

Particle clustering has been shown to significantly change the SLP of monodisperse nanoparticles. However, the effect of clustering is so dependent on particle diameter that one can ask whether in polydisperse systems a modulation of thermal efficiency is still possible. Only the case of SLP enhancement is considered here. We have

explored the variation of W_{SLP} for clustering particles distributed in size according to a gaussian distribution function $p(D)$ (some examples are shown in the right panel of Figure 7). Particles of different diameter are assumed to randomly occupy the sites on the simple cubic lattice representing the homogeneous particle distribution. The average interparticle distance is now $\overline{d_0} = \overline{V}/f_V$ where $\overline{V}$ is the average particle volume. The energy barrier of each particle is modified by the expression of E_D given in Equation 4.

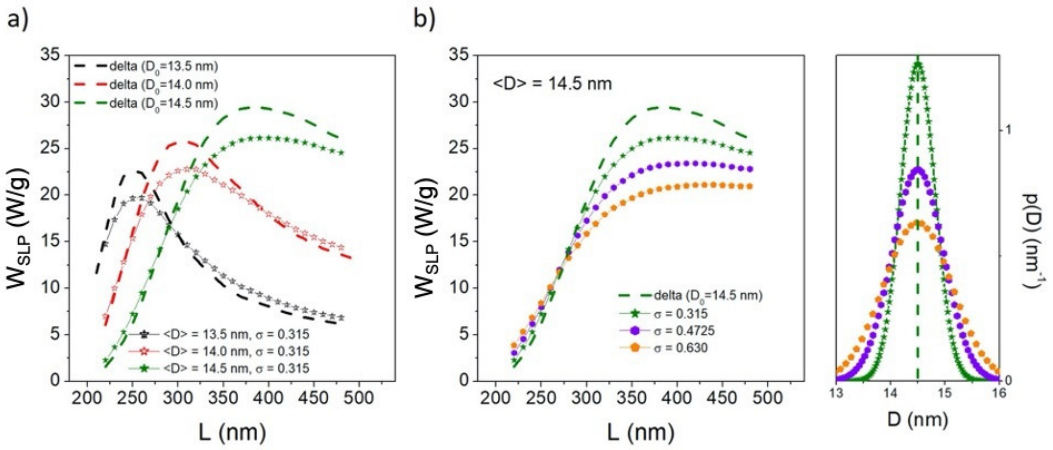

Figure 7. Panel a): effect of a narrow Gaussian distribution of magnetite particle sizes around three values of D on the behaviour of the SLP with the size of clusters (for $N = 10$); the dashed lines apply to the corresponding monodisperse systems. Panel b): smoothing effect of an increasing standard deviation of the Gaussian distribution centred at $D = 14.5$ nm. The Gaussian functions used in panels a) and b) are shown in the rightmost panel.

The results are reported in Figure 7. The effect of a narrow gaussian distribution with standard deviation $\sigma = 0.315$ nm centred at three different values of D is shown in panel a along with the curves obtained in the corresponding monodisperse particles (dashed lines). Therefore, a narrow $p(D)$ function preserves the main features of the enhancement of the W_{SLP} parameter induced by particle clustering. It should be noted that the present value of σ corresponds to a range of particle sizes in the 13.5 -15.5 nm interval (see green curve in the right panel), i.e., a range of about 2 nm which is compatible with the requirements for hyperthermia-based therapy [7, 72], where however the conceptual aim is to deal with an even narrower dispersion of particle sizes. An example of the smoothing effect observed by increasing the standard deviation of $p(D)$ is shown in panel b of Figure 7, where the $W_{SLP}(d)$ curves corresponding to the delta function and to three gaussian distributions, all peaked at $D = 14.5$ nm, are reported. The colours correspond to the σ values reported in the centre panel. Of course, the larger σ, the smoother and featureless is the $W_{SLP}(d)$ curve. Generally speaking, beneficial effects of particle clustering on thermal efficiency clearly emerge when the particle distribution function is sufficiently narrow.

4. Conclusion

The formation of dense clusters of magnetite nanoparticles significantly modifies their heating efficiency with respect to the homogeneous dispersion. The effect is dominated by dipole-dipole interaction which can become particularly strong inside a cluster because of the lower mean interparticle distance. This results in an increase of the energy barrier which has to be overcome by the magnetization of a particle.

A simple idealized model of magnetic clusters has been developed. The effect of intra-cluster dipolar interactions on the shape of minor hysteresis loops turns out to be critically dependent on particle size. As a consequence, clustering of small magnetite nanoparticles ($D \lesssim 14$ nm) leads to a significant enhancement of the specific loss power, and clustering of large particles ($D \gtrsim 15$ nm) reduces their ability to heat. In other words, large particles are more efficient as heaters when they are homogeneously distributed in a host medium, whereas dense clusters comprised of small particles have a definitely higher SLP than the corresponding homogeneous dispersions. This circumstance can be exploited to produce suitable nanoparticle preparations intended either to enhance the thermal efficiency of magnetic particles (a property sought after in such distant application areas as magnetic hyperthermia for anti-cancer therapy and flow assurance in oil production and transport), or to reduce the undesired heating of tissues as in Magnetic Particle Imaging.

The particle size ensuring the best modulation ability of the SLP is $D \approx 14$ nm: in this case, the formation of clusters of proper size can either increase or decrease the SLP, which would permit to prepare multi-purpose nanomaterials (e.g., ferrofluids) tailored for specific applications.

In polydisperse systems, the contrasting effects of dipolar interactions in particles of different size tend to counterbalance, therefore reducing the effect of particle clustering on the SLP. However, narrow size distributions as the ones used in magnetic hyperthermia still retain most of the features observed in monodisperse particle systems.

This model permits to freely modify all parameters playing a role in the process of cyclic magnetization, so that one can easily interpret the magnetic behaviour of a nanoparticle system and draw a comprehensive, self consistent picture of the resulting effects with a predictive character that may escape other approaches.

In conclusion, dipole-dipole interaction among particles is particularly sensitive to the degree of uniformity of the particle distribution in a host material or a tissue. This property can be used in a variety of applications by creating compact clusters where the individual particles are physically kept separated from each other, e.g., by a diamagnetic coating. Clusters of this type are characterized by a very different magnetic behaviour and efficiency in the release of thermal energy with respect to homogeneous dispersions. The volume of real compact particle clusters (comprised of $\sim 10^3 \div 10^5$ individual particles) is much smaller than the one of a typical target in a living body (of the order of the cubic centimeter), so that each cluster can still be safely considered to be a "point-

like" heat source on the macroscopic scale; in the case of clustering, a non-homogeneous distribution of heat on the nanometer scale is expected; however, heat is transferred in a living body non only by thermal diffusion but also, and more efficiently, by convection through the blood flow, so that a uniform temperature is expected to be quickly achieved everywhere in the target volume even in the presence of a non-homogeneous distribution of individual particles.

The effects studied in the present paper should be properly taken into account in the efforts towards the optimization of all applications involving high-frequency magnetization processes of magnetic particles.

References

[1] Thanh N T K 2018 *Clinical Applications of Magnetic Nanoparticles: From Fabrication to Clinical Applications* ed N T K Thanh (CRC Press)

[2] Zhou K, Zhou X, Liu J and Huang Z 2020 Application of magnetic nanoparticles in petroleum industry: A review *J. Pet. Sci. Eng.* **188** 106943

[3] Haseeb Q, Hamdani S D A, Akram A, Khan D A, Rajput T A and Babar M M 2020 *Nanobiotechnology: Paving the Way to Personalized Medicine NanoBioMedicine* (Springer Singapore) pp 17–32

[4] Périgo E A, Hemery G, Sandre O, Ortega D, Garaio E, Plazaola F and Teran F J 2015 Fundamentals and advances in magnetic hyperthermia *Appl. Phys. Rev.* **2** 1–35

[5] Bakenecker A, Ahlborg M, Debbeler C, Kaethner C and Lüdtke-Buzug K 2018 *Magnetic Particle Imaging Precision Medicine: Tools and Quantitative Approaches* (Elsevier Inc.) pp 183–228

[6] Sengul A B and Asmatulu E 2020 Toxicity of metal and metal oxide nanoparticles: a review *Environ. Chem. Lett.* **18** 1659–83

[7] Beola L, Gutiérrez L, Grazú V and Asín L 2019 A Roadmap to the Standardization of In Vivo Magnetic Hyperthermia *Nanomaterials for Magnetic and Optical Hyperthermia Applications* ed R M Fratila and J M De La Fuente (Elsevier Ltd) pp 317–37

[8] Allia P, Barrera G and Tiberto P 2019 Nonharmonic Driving Fields for Enhancement of Nanoparticle Heating Efficiency in Magnetic Hyperthermia *Phys. Rev. Appl.* **12** 034041

[9] Barrera G, Allia P and Tiberto P 2020 Fine tuning and optimization of magnetic hyperthermia treatments using versatile trapezoidal driving-field waveforms *Nanoscale Adv.* **2** 4652-4664

[10] Dutz S and Hergt R 2013 Magnetic nanoparticle heating and heat transfer on a microscale: Basic principles, realities and physical limitations of hyperthermia for tumour therapy *Int. J. Hyperth.* **29** 790–800

[11] Negut I and Grumezescu V 2019 *Nanoparticles and hyperthermia* (Elsevier Inc.)

[12] Marino A, Camponovo A, Degl'Innocenti A, Bartolucci M, Tapeinos C, Martinelli C, De Pasquale D, Santoro F, Mollo V, Arai S, Suzuki M, Harada Y, Petretto A and Ciofani G 2019 Multifunctional temozolomide-loaded lipid superparamagnetic nanovectors: Dual targeting and disintegration of glioblastoma spheroids by synergic chemotherapy and hyperthermia treatment *Nanoscale* **11** 21227–48

[13] Ding J, Chen J, Gao L, Jiang Z, Zhang Y, Li M, Xiao Q, Lee S S and Chen X 2019 Engineered nanomedicines with enhanced tumor penetration *Nano Today* **29** 100800

[14] Talebloo N, Gudi M, Robertson N and Wang P 2020 Magnetic Particle Imaging: Current Applications in Biomedical Research *J. Magn. Reson. Imaging* **51** 1659–68

[15] Knopp T, Gdaniec N and Möddel M 2017 Magnetic particle imaging: From proof of principle to preclinical applications *Phys. Med. Biol.* **62** R124–78

[16] Wells J, Paysen H, Kosch O and Wiekhorst F 2020 Heat dissipation and safety considerations during lissajous scanning magnetic particle imaging *Int. J. Magn. Part. Imaging* **6** 1–3

[17] Chen H, Kaminski M D, Liu X, Mertz C J, Xie Y, Torno M D and Rosengart A J 2007 A novel human detoxification system based on nanoscale bioengineering and magnetic separation techniques *Med. Hypoth.* **68** 1071–1079

[18] Chen H, Ebner A D, Ritter J A, Kaminsku M D and Rosengart A J 2008 Theoretical Analysis of a Magnetic Separator Device for Ex-Vivo Blood Detoxification *Separ. Sci. Technol.* **43** 996-1020

[19] Stamopoulos D, Bouziotis P, Benaki D, Kotsovassilis C and Zirogiannis P N 2008 Utilization of nanobiotechnology in haemodialysis: mock-dialysis experiments on homocysteine *Nephrol. Dial. Transplant.* **23** 3234-3239

[20] Stamopoulos D, Manios E, Gogola V, Benaki D, Bouziotis P, Niarchos D and Pissas M 2008 Bare and protein-conjugated Fe_3O_4 ferromagnetic nanoparticles for utilization in magnetically assisted hemodialysis: biocompatibility with human blood cells *Nanotechnology* **51** 505101

[21] Stamopoulos D, Gogola V, Manios E, Gourni E, Benaki D, Niarchos D and Pissas M 2009 Biocompatibility and Solubility of Fe_3O_4-BSA Conjugates with Human Blood *Curr. Nanosci.* **5** 177-181

[22] Moersdorf D, Hugounenq P, Phuoc L T, Mamlouk-Chaouachi H, Felder-Flesch D, Begin-Colin S, Pourroy G and Bernhardt I 2010 *Adv. Biosci. Biotechnol.* **1** 439-443

[23] Rodrigues R O, Bañobre-López M, Juan Gallo J, Tavares P B, Silva A M T, Lima R and Gomes H T 2016 Haemocompatibility of iron oxide nanoparticles synthesized for theranostic applications: a high-sensitivity microfluidic tool *J. Nanopart. Res.* **18** 194

[24] Nosrati H, Salehiabar M, Fridoni M, Abdollahifar M A, Manjili H K, Davaran S and Danafar H 2019 New Insight about Biocompatibility and Biodegradability of Iron Oxide Magnetic Nanoparticles: Stereological and In Vivo MRI Monitor *Sci. Reports* **9** 7173

[25] Karageorgou M A, Bouziotis P, Vranješ-Djurić S and Stamopoulos D 2020 Hemocompatibility of gallium-68 labeled iron oxide nanoparticles coated with 2,3-dicarboxypropane-1,1-diphosphonic acid *Mat. Sci. Eng. C* **115** 111121

[26] Shingala J, Shah V, Dudhat K and Shah M 2020 Evolution of nanomaterials in petroleum industries: application and the challenges *J. Pet. Explor. Prod. Technol.* **10** 3993–4006

[27] Rosenweig R E 2002 Heating magnetic fluid with alternating magnetic fiel *J. Magn. Magn. Mater.* **252** 370–2

[28] Lahiri B B, Ranoo S and Philip J 2017 Uncertainties in the estimation of specific absorption rate during radiofrequency alternating magnetic field induced non-adiabatic heating of ferrofluids *J. Phys. D. Appl. Phys.* **50** 455005

[29] Wildeboer R R, Southern P and Pankhurst Q A 2014 On the reliable measurement of specific absorption rates and intrinsic loss parameters in magnetic hyperthermia materials *J. Phys. D. Appl. Phys.* **47** 495003

[30] Wells J, Kazakova O, Posth O, Steinhoff U, Petronis S, Bogart L K, Southern P, Pankhurst Q and Johansson C 2017 Standardisation of magnetic nanoparticles in liquid suspension *J. Phys. D. Appl. Phys.* **50** 383003

[31] Makridis A, Curto S, Van Rhoon G C, Samaras T and Angelakeris M 2019 A standardisation protocol for accurate evaluation of specific loss power in magnetic hyperthermia *J. Phys. D. Appl. Phys.* **52** 255001

[32] Shasha C and Krishnan K M 2020 Nonequilibrium Dynamics of Magnetic Nanoparticles with Applications in Biomedicine *Adv. Mater.* **1904131** 48–50

[33] Lartigue L, Hugounenq P, Alloyeau D, Clarke S P, Lévy, Michael, Bacri J-C, Bazzi R, Brougham D F, Wilhelm C and Gazeau F 2012 Cooperative Organization in Iron Oxide Multi-Core Nanoparticles Potentiates Their Efficiency as Heating Mediators and MRI Contrast Agents *ACS Nano* **6** 10935–49

[34] Herman K, Lang M E and Pich A 2018 Tunable clustering of magnetic nanoparticles in microgels: Enhanced magnetic relaxivity by modulation of network architecture *Nanoscale* **10** 3884–92

[35] Li Y, Hu K, Chen B, Liang Y, Fan F, Sun J, Zhang Y and Gu N 2017 Fe_3O_4@PSC nanoparticle clusters with enhanced magnetic properties prepared by alternating-current magnetic field

assisted co-precipitation *Colloids Surfaces A Physicochem. Eng. Asp.* **520** 348–54
[36] Shen S, Wang S, Zheng R, Zhu X, Jiang X, Fu D and Yang W 2015 Magnetic nanoparticle clusters for photothermal therapy with near-infrared irradiation *Biomaterials* **39** 67–74
[37] Togashi T, Naka T, Asahina S, Sato K, Takami S and Adschiri T 2011 Surfactant-assisted one-pot synthesis of superparamagnetic magnetite nanoparticle clusters with tunable cluster size and magnetic field sensitivity *Dalt. Trans.* **40** 1073–8
[38] Turcu R, Socoliuc V, Craciunescu I, Petran A, Paulus A, Franzreb M, Vasile E and Vekas L 2015 Magnetic microgels, a promising candidate for enhanced magnetic adsorbent particles in bioseparation: Synthesis, physicochemical characterization, and separation performance *Soft Matter* **11** 1008–18
[39] Pearce J, Giustini A, Stigliano R and Hoopes P J 2013 Magnetic heating of nanoparticles: The importance of particle clustering to achieve therapeutic temperatures *J. Nanotechnol. Eng. Med.* **4** 0110071-01100714
[40] Roveimiab Z, Mahdavian A R, Biazar E and Heidari K S 2012 Preparation of Magnetic Chitosan Nanocomposite Particles and Their Susceptibility for Cellular Separation Applications *J. Colloid Sci. Biotechnol.* **1** 82–8
[41] Yang Qu, Jianbo Li, Jie Ren, Junzhao Leng, Chao Lin and D S 2014 Enhanced Magnetic Fluid Hyperthermia by Micellar *Magnetic Appl. Mater. Interfaces* **6** 16867–16879
[42] Usov N A, Serebryakova O N and Tarasov V P 2017 Interaction Effects in Assembly of Magnetic Nanoparticles *Nanoscale Res. Lett.* **12** 489
[43] Fu R, Yan Y, Roberts C, Liu Z and Chen Y 2018 The role of dipole interactions in hyperthermia heating colloidal clusters of densely-packed superparamagnetic nanoparticles *Sci. Rep.* **8** 1–10
[44] Allia P, Barrera G and Tiberto P 2020 Hysteresis effects in magnetic nanoparticles: A simplified rate-equation approach *J. Magn. Magn. Mater.* **496** 165927
[45] Barrera G, Allia P and Tiberto P 2021 Dipolar Interactions Among Magnetite Nanoparticles For Magnetic Hyperthermia: A Rate-Equation Approach *Nanoscale* Accepted Manuscript https://doi.org/10.1039/D0NR07397K
[46] Dormann J L, Fiorani D and Tronc E 1999 On the models for interparticle interactions in nanoparticle assemblies: comparison with experimental results *J. Magn. Magn. Mater.* **202** 251–67
[47] Barrera G, Allia P and Tiberto P 2020 Temperature-dependent heating efficiency of magnetic nanoparticles for applications in precision nanomedicine *Nanoscale* **12** 6360–77
[48] Usov N A 2011 Numerical simulation of field-cooled and zero field-cooled processes for assembly of superparamagnetic nanoparticles with uniaxial anisotropy *J. Appl. Phys.* **109** 023913
[49] Soukup D, Moise S, Céspedes E, Dobson J and Telling N D 2015 In Situ Measurement of Magnetization Relaxation of Internalized Nanoparticles in Live Cells *ACS Nano* **9** 231–40
[50] Usov N A and Serebryakova O N 2020 Equilibrium properties of assembly of interacting superparamagnetic nanoparticles *Sci. Rep.* **10** 1–14
[51] Morup S 1994 Superparamagnetism and Spin Glass Ordering in Magnetic Nanocomposites *Europhys. Lett.* **28** 671–6
[52] Moya C, Iglesias Ó, Batlle X and Labarta A 2015 Quantification of Dipolar Interactions in $Fe_{3-x}O_4$ Nanoparticles *J. Phys. Chem. C* **119** 24142–8
[53] Ruta S, Chantrell R and Hovorka O 2015 Unified model of hyperthermia via hysteresis heating in systems of interacting magnetic nanoparticles *Sci. Rep.* **5** 1–7
[54] Brown W F 1963 Thermal fluctuations of a single-domain particle *Phys. Rev.* **130** 1677–86
[55] Jeon S, Hurley K R, Bischof J C, Haynes C L and Hogan C J 2016 Quantifying intra- and extracellular aggregation of iron oxide nanoparticles and its influence on specific absorption rate *Nanoscale* **8** 16053–64
[56] Lisjak D and Mertelj A 2018 Anisotropic magnetic nanoparticles: A review of their properties, syntheses and potential applications *Prog. Mater. Sci.* **95** 286–328
[57] Fiorani D and Peddis D 2014 Understanding dynamics of interacting magnetic nanoparticles: From

the weak interaction regime to the collective superspin glass state *Journal of Physics: Conference Series vol 521 (Institute of Physics Publishing)* **521** 012006

[58] Rivas Rojas P C, Tancredi P, Moscoso Londoño O, Knobel M and Socolovsky L M 2018 Tuning dipolar magnetic interactions by controlling individual silica coating of iron oxide nanoparticles *J. Magn. Magn. Mater.* **451** 688–96

[59] Cuchillo A, Rivas-Rojas P, Tancredi P, Socolovsky L M and Vargas P 2020 Combining dipolar and anisotropic contributions to properly describe the magnetic properties of magnetic nanoparticles real systems *J. Magn. Magn. Mater.* **508** 166842

[60] Cullity B D and Graham C D 2009 *Introduction to Magnetic Materials*

[61] Anand M, Carrey J and Banerjee V 2012 Spin morphologies and heat dissipation in spherical assemblies of magnetic nanoparticles *Phys.Rev.B* **94** 094425

[62] Kuznetsov A A 2019 Zero-Field and Field-Induced Interactions between Multicore Magnetic Nanoparticles *Nanomater.* **9** 718

[63] Lattuada M 2019 Effect of Clustering on the Heat Generated by Superparamagnetic Iron Oxide Nanoparticles *Chimia* **73** 39-42

[64] Fu R, Yan Y Y and Roberts C 2015 Study of the effect of dipole interactions on hyperthermia heating the cluster composed of superparamagnetic nanoparticles *AIP Advances* **5** 127232

[65] Bender P, Wetterskog E, Honecker D, Fock J, Frandsen C, Moerland C, Bogart L K, Posth O., Szczerba W, Gavilán H, Costo R, Fernández-Díaz M T, González-Alonso D, Fernández Barquín L and Johansson C. 2018 Dipolar-coupled moment correlations in clusters of magnetic nanoparticles *Phys.Rev.* B **98** 224420

[66] Anand M 2021 Hysteresis in Two Dimensional Arrays of Magnetic Nanoparticles, arXiv:2104.02961v1 [cond-mat.mtrl-sci] 7 Apr 2021

[67] Pearce J, Giustini A, Stigliano R and Hoopes P J 2014 Magnetic Heating of Nanoparticles: The Importance of Particle Clustering to Achieve Therapeutic Temperatures *J. Nanotech. Engin. and Med.* **4** 011007

[68] Halgamuge M N and Song T 2020 Optimizing Heating Efficiency of Hyperthermia: Specific Loss Power of Magnetic Sphere Composed of Superparamagnetic Nanoparticles *Progr. Electromagn. Res. B* **87** 1-17

[69] Wang C, Hsu C H, Li Z, Hwang L P, Lin Y C, Chou P T and Lin Y Y 2017 E ffective heating of magnetic nanoparticle aggregates for in vivo nano-theranostic hyperthermia *Int. J. Nanomed.* **I2** 6273-6287

[70] Tang Y, Jin T and Flesch R C C 2017 Numerical temperature analysis of magnetic hyperthermia considering nanoparticle clustering and blood vessels Tang Y, Jin T and Flesch R C C 2017 Numerical temperature analysis of magnetic hyperthermia considering nanoparticle clustering and blood vessels *IEEE Trans. Magnetics* **53** 5400106

[71] Stylianopoulos T *Eur. J. Nanomed.* 2016 Intelligent drug delivery systems for the treatment of solid tumors *Eur. J. Nanomed.* **8** 9

[72] Maier-Hauff K, Ulrich F, Nestler D, Niehoff H, Wust P, Thiesen B, Orawa H, Budach V and Jordan A 2011 Efficacy and safety of intratumoral thermotherapy using magnetic iron-oxide nanoparticles combined with external beam radiotherapy on patients with recurrent glioblastoma multiforme *J. Neurooncol.* **103** 317–24